Introduction to Cosmic Ray Detectors

Jose Bellido

Third School of Cosmic Rays and Astrophysics

August 25th to September 5th , 2008

Arquipa - Peru

Outline

-Introduction to Cosmic Rays

-Observation Techniques at Various Energies

-Detectors for the Highest Energy Cosmic Rays

History of Cosmic Rays Research

Cosmic rays research started after studies of the electrical conductive properties in gases.

- In Paris in 1785 C.A. de Coulomb reported that any thing charged would loss gradually its charge (despite a careful insulation) in some mysterious way. No clear explanation was found.

- Around 1900 Elster and Geitel in Berlin deduced that electrical conduction in air resulted from the presence of positive and negative ions on the air.

- C. Wilson (1901) found that an ionic current can persist even in a sealed volume of gas. How ions are continuously regenerating? Wilson suggested that the ionization in a closed vessel may be due to an extra-terrestrial radiation penetrating the atmosphere of the earth. Unfortunately he could not prove it and later gave up his hypothesis.

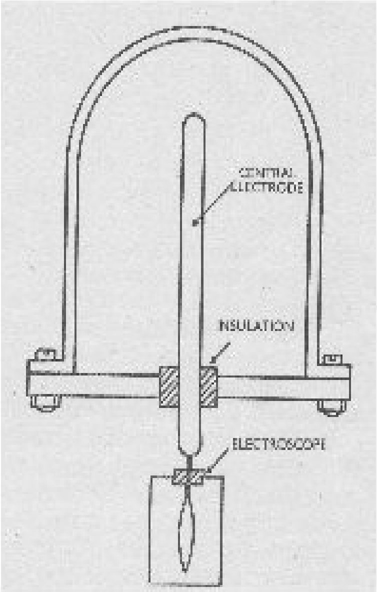

Rutherford and Cook proved that radiation was coming from outside the chamber. The rate of ionization was reduced by surrounding the chamber with absorbers of lead. It became more or less accepted that all the "penetrating radiation" came from natural radiation in the earth.

- Certain amount of ionization persisted even above see water, and ionization above sea varied with the barometric pressure. This contradicted the terrestrial origin.

Viktor F. Hess in 1912 made the great breakthrough

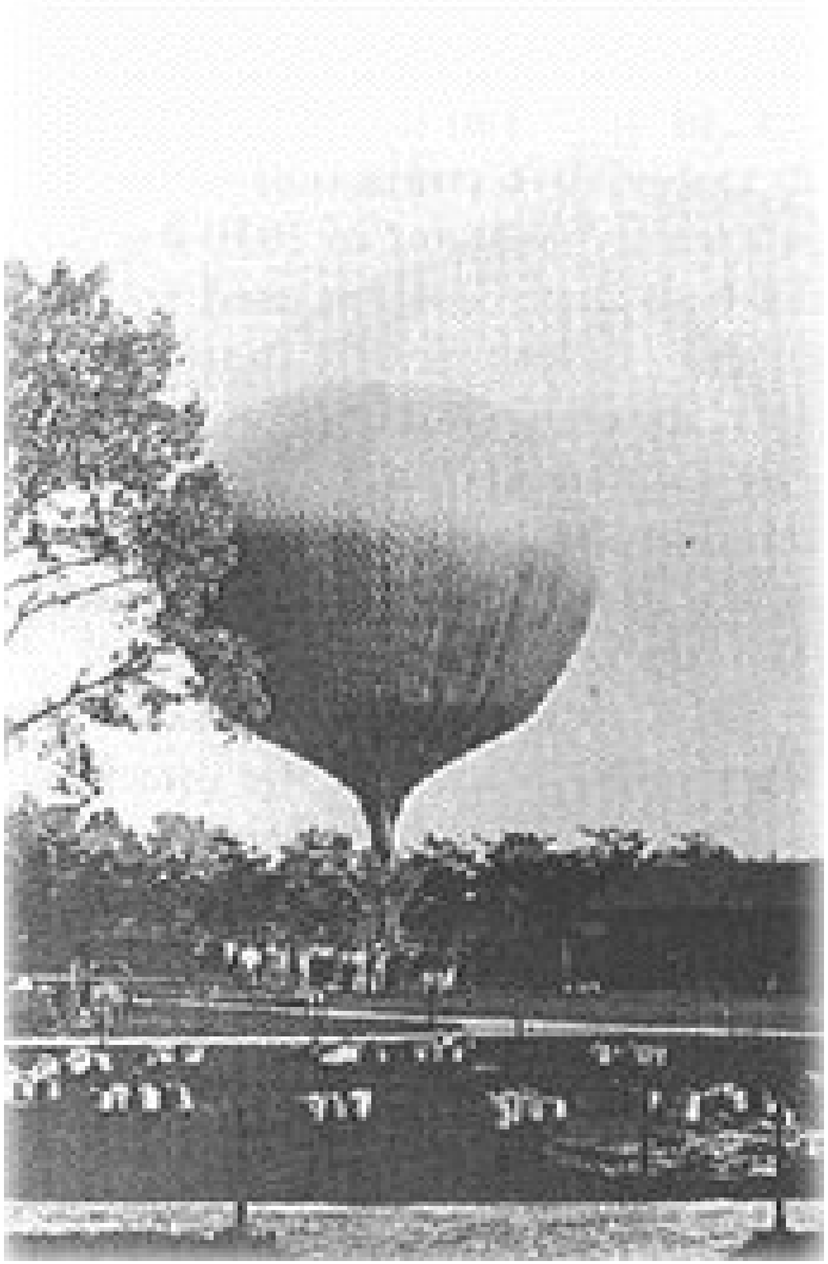

Hess measured the ionization rate at different atmospheric altitudes up to 5 km.

TABLE OF MEAN VALUES

Mean height above ground m	Observed radiation in ions per cc per sec			
	Inst. 1	Inst. 2	Inst. 3	
	q_1	q_2	q_3 red.	q_3 not red.
0	16·3 (18)	11·8 (20)	19·6 (9)	19·7 (9)
up to 200	15·4 (13)	11·1 (12)	19·1 (8)	18·5 (8)
200– 500	15·5 (6)	10·4 (6)	18·8 (5)	17·7 (5)
500–1000	15·6 (3)	10·3 (4)	20·8 (2)	18·5 (2)
1000–2000	15·9 (7)	12·1 (8)	22·2 (4)	18·7 (4)
2000–3000	17·3 (1)	13·3 (1)	31·2 (1)	22·5 (1)
3000–4000	19·8 (1)	16·5 (1)	35·2 (1)	21·8 (1)
4000–5200	34·4 (2)	27·2 (2)	—	—

Hess measurements showed that some radiation was coming from above the atmosphere.

- Milikan with a different experiment in 1925 definitely confirmed Hess results. Milikan introduced the name “cosmic rays”.

Cosmic Ray studies gave origin to a new field in physics "Particle Physics"

TABLE 3.2. THE DISCOVERY OF THE ELEMENTARY PARTICLES

This table, an expansion of one given by Powell, Fowler and Perkins (1959), shows how and when the relatively stable elementary particles were discovered (antiparticles being included somewhat arbitrarily). The heavy lines show the discoveries made using cosmic rays. The particles are listed in order of increasing mass, except within charge multiplets.

Date: 1900, 1930, 1931, 1932, 1933, 1934, 1935, 1936, 1937, 1938, 1939, 1940, 1941, 1942, 1943, 1944, 1945, 1946, 1947, 1948, 1949, 1950, 1951, 1952, 1953, 1954, 1955, 1956, 1957, 1958, 1959, 1960, 1961, 1962, 1963, 1964, 1965, 1966, 1967

Particle	Source of radiation	Instrument used	Specific observation made
$\bar{\nu}_e(\nu_e)$	nuclear reactor	liquid scintillator	Capture by proton
ν_μ	accelerator	spark chamber	Production of μ and not e
e^-	discharge tube	fluorescent screen	Ratio e/m
e^+	cosmic rays	cloud chamber	Charge, mass
μ^+, μ^-	cosmic rays	cloud chamber	Absence of radiation loss in Pb; decay at rest; mass
π^+	cosmic rays	nuclear emulsion	$\pi-\mu$ decay at rest
π^-	cosmic rays	nuclear emulsion	Nuclear interaction at rest
π^0	accelerator	counters	Decay into γ-rays
K^+	cosmic rays	nuclear emulsion	$K_{\pi 3}$ decay
K^-	cosmic rays	nuclear emulsion	Nuclear interaction at rest
K^0	cosmic rays	cloud chamber	Decay into $\pi^+\pi^-$ in flight
η	accelerator	bubble chamber	Total mass of decay products
p	discharge tube	spectroscopes; mass spectrometers	Charges and masses of ions
$\bar{p}$	accelerator	Cerenkov counter	e/m measured; annihilation
n	radioactivity	ionization chamber	Mass from elastic collisions
$\bar{n}$	accelerator	counters	Annihilation
Λ	cosmic rays	cloud chamber	Decay to $p\pi^-$ in flight
$\bar{\Lambda}$	accelerator	nuclear emulsion	Decay to $\bar{p}\pi^+$ in flight
Σ^+	cosmic rays	nuclear emulsion	Decay at rest
Σ^-	accelerator	diffusion chamber	Decay to $n\pi^-$ in flight
Σ^0	accelerator	bubble chamber	Decay to $\Lambda\gamma$ in flight
Ξ^-	cosmic rays	cloud chamber	Decay to $\Lambda\pi^-$ in flight
Ξ^0	accelerator	bubble chamber	Decay to $\Lambda\pi^0$ in flight
Ω^-	accelerator	bubble chamber	Decay to $\Xi^0\pi^-$ in flight
Very many "resonance" particles with lifetimes $\sim 10^{-23}$ to 10^{-19} s	accelerator	bubble chambers	Total mass of decay products
?"Fireballs"	cosmic rays	nuclear emulsion	Angles of meson emission
Quarks?	not found with accelerators; being sought in cosmic rays		Charge $\frac{1}{3}$ or $\frac{2}{3}e$

Cosmic Ray Characteristics

- Mass Composition
- Energy Spectrum
- Arriving Directions

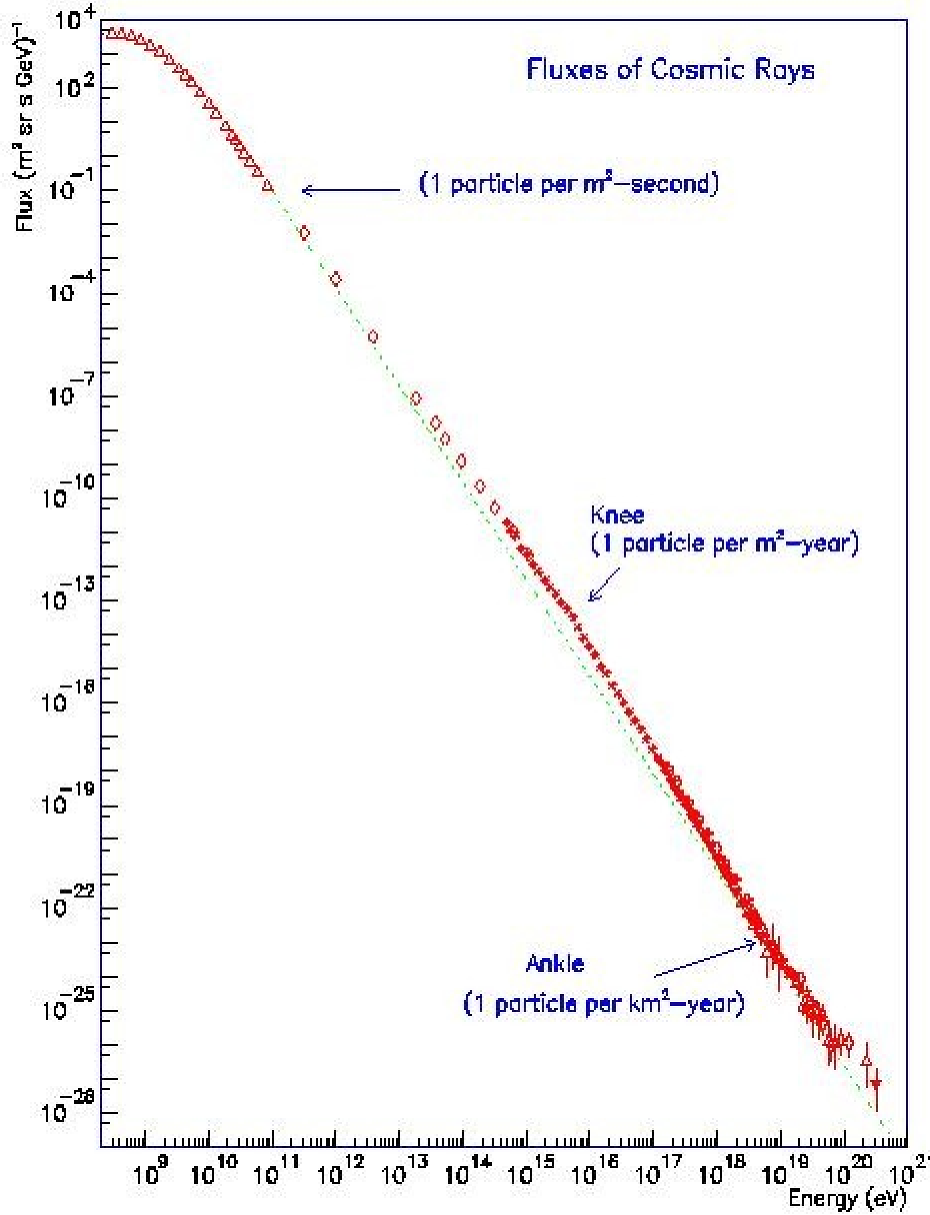

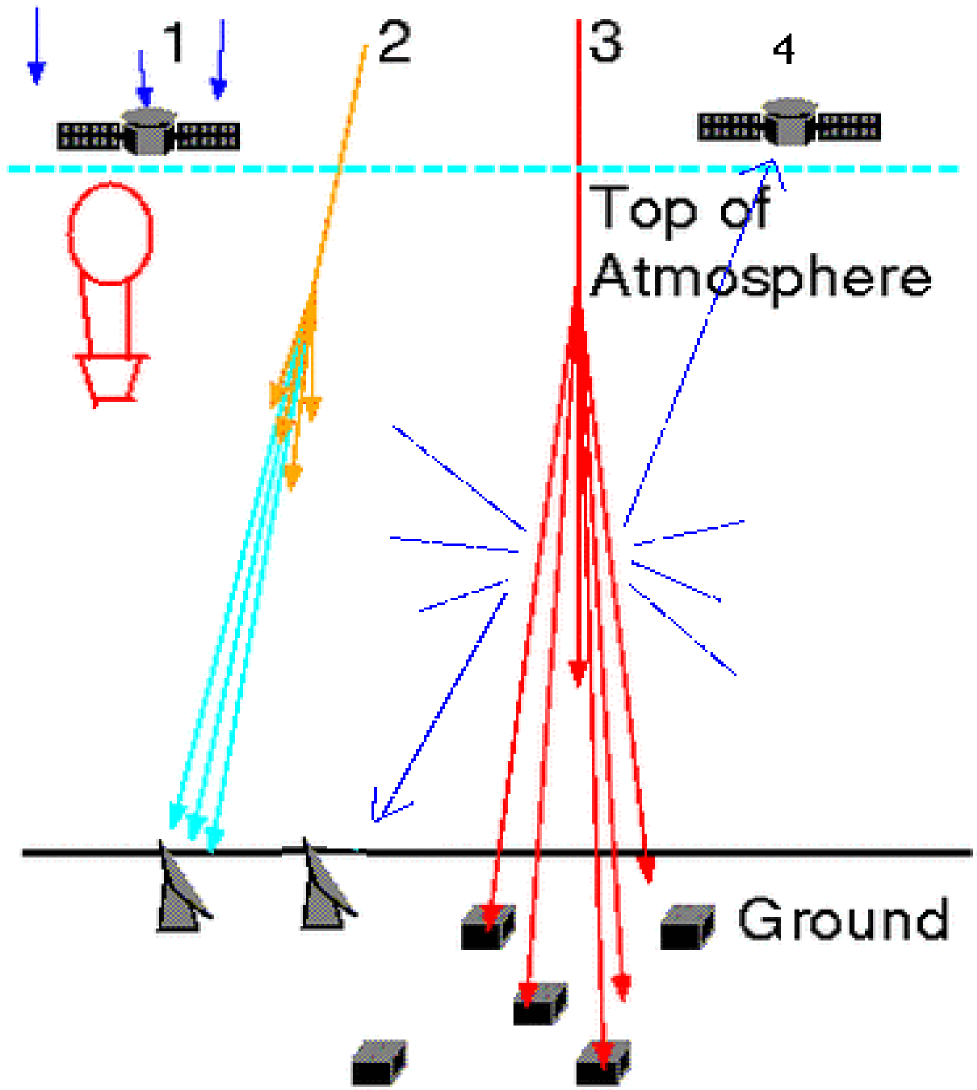

- Region 1: May go up to 10^{14} eV.
- Region 2: around 10^{12} eV, (especially for TeV gama rays).
- Region 3:From ≈ 10^{12} eV to the highest energies.
- Region 4:Especially above 10^{19} eV.

Energetic Cosmic Rays Interacting with the Atmosphere

Energetic CR (protons, nuclei, photons or neutrinos) coming from out space interact at the top of our atmosphere. In this interaction they create secondary particles. These secondary particles are also energetic and can continue creating more secondary particles generating an **extensive air shower (EAS).** When the secondary particles are not anymore energetic enought to generate more particles, the air shower reaches its maximum size (**shower maximum**). From that point forward the number of particles in the air shower starts to decrease.

Extensive Air Shower

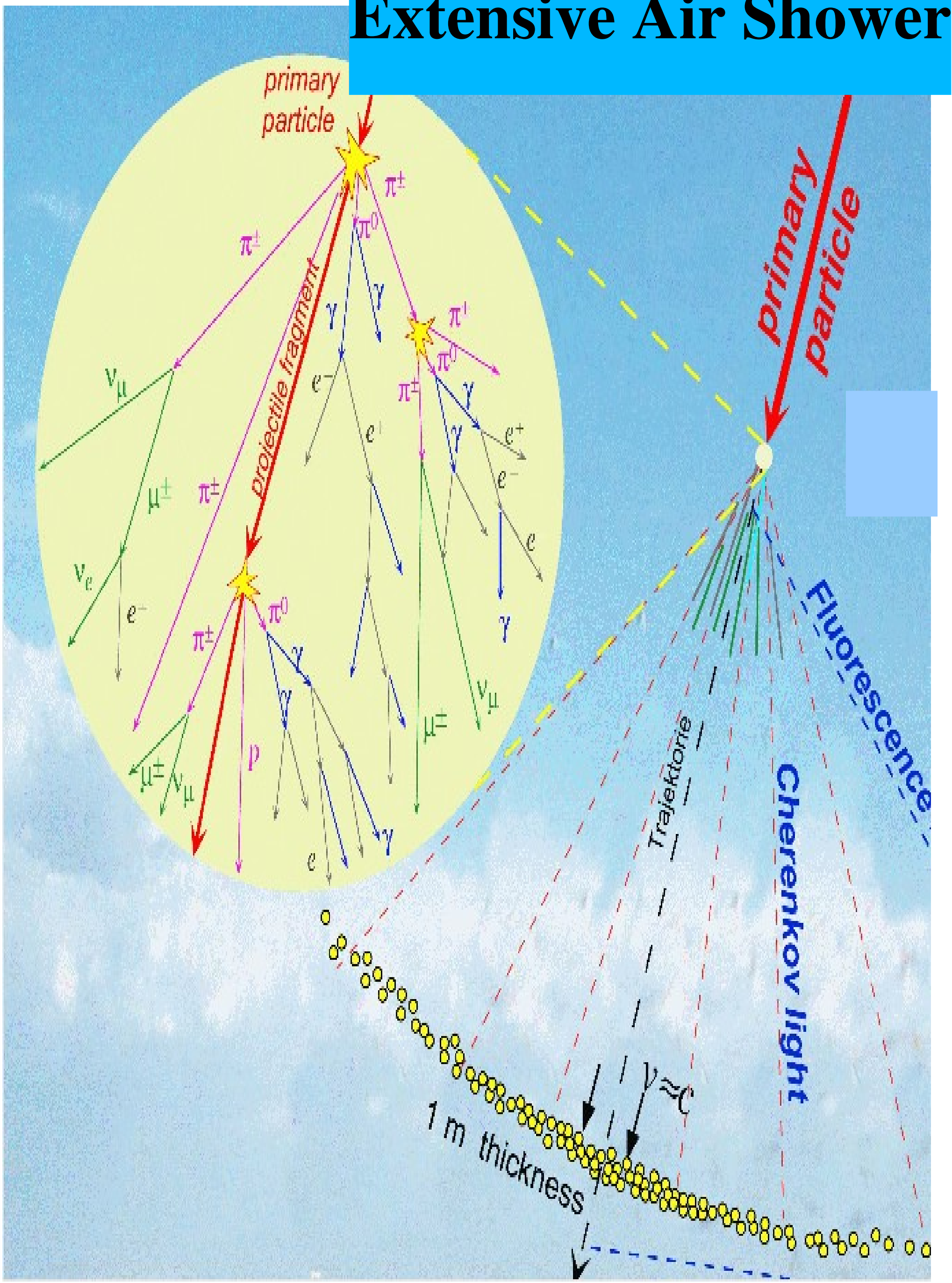

Detectores de Superficie y Detectores de Fluorescencia

(The Pierre Auger Observatory)

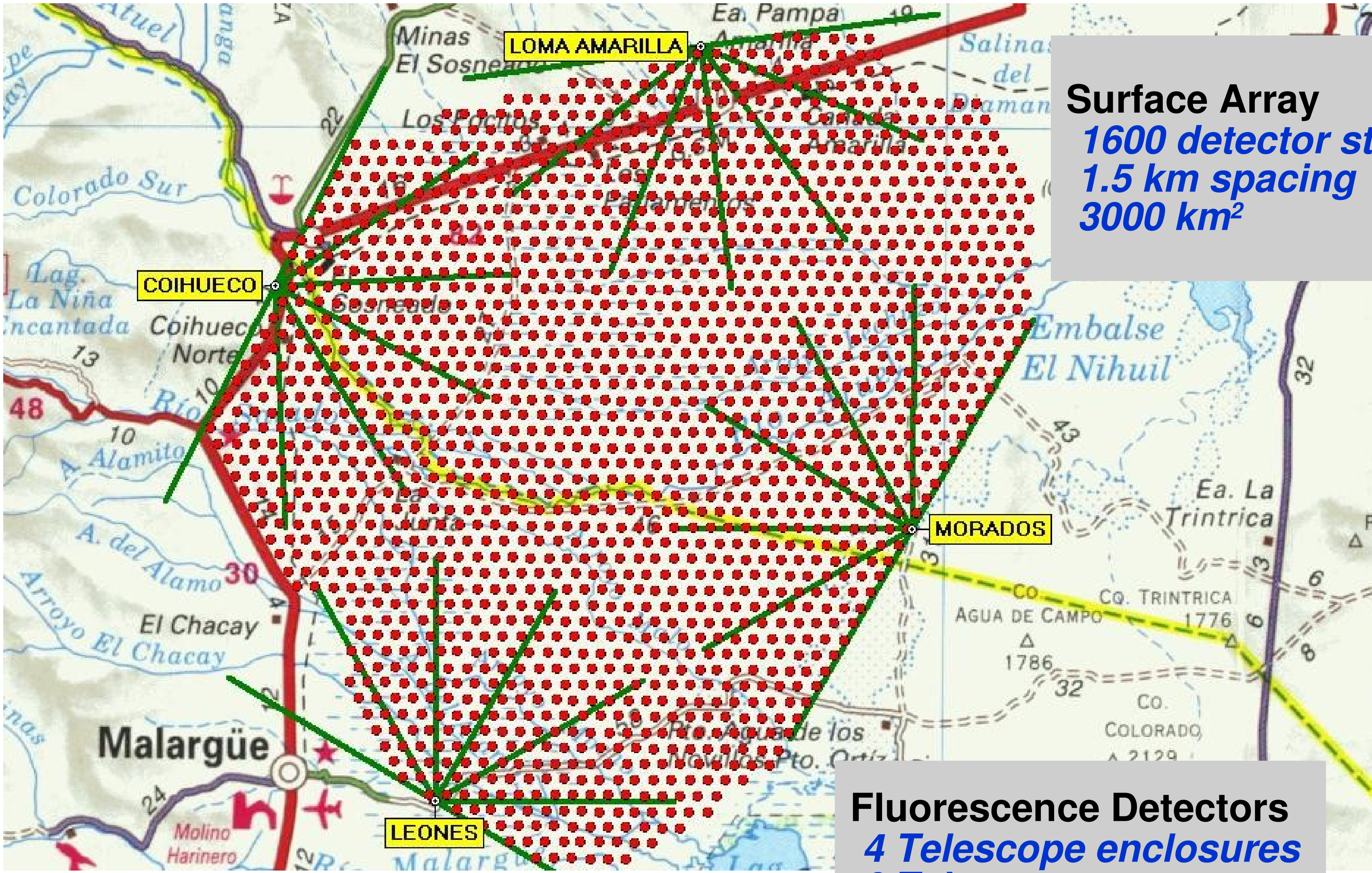

Surface Array

1600 detector stations
1.5 km spacing
3000 km^2

Fluorescence Detectors

4 Telescope enclosures
6 Telescopes per enclosure
24 Telescopes total


EZRA

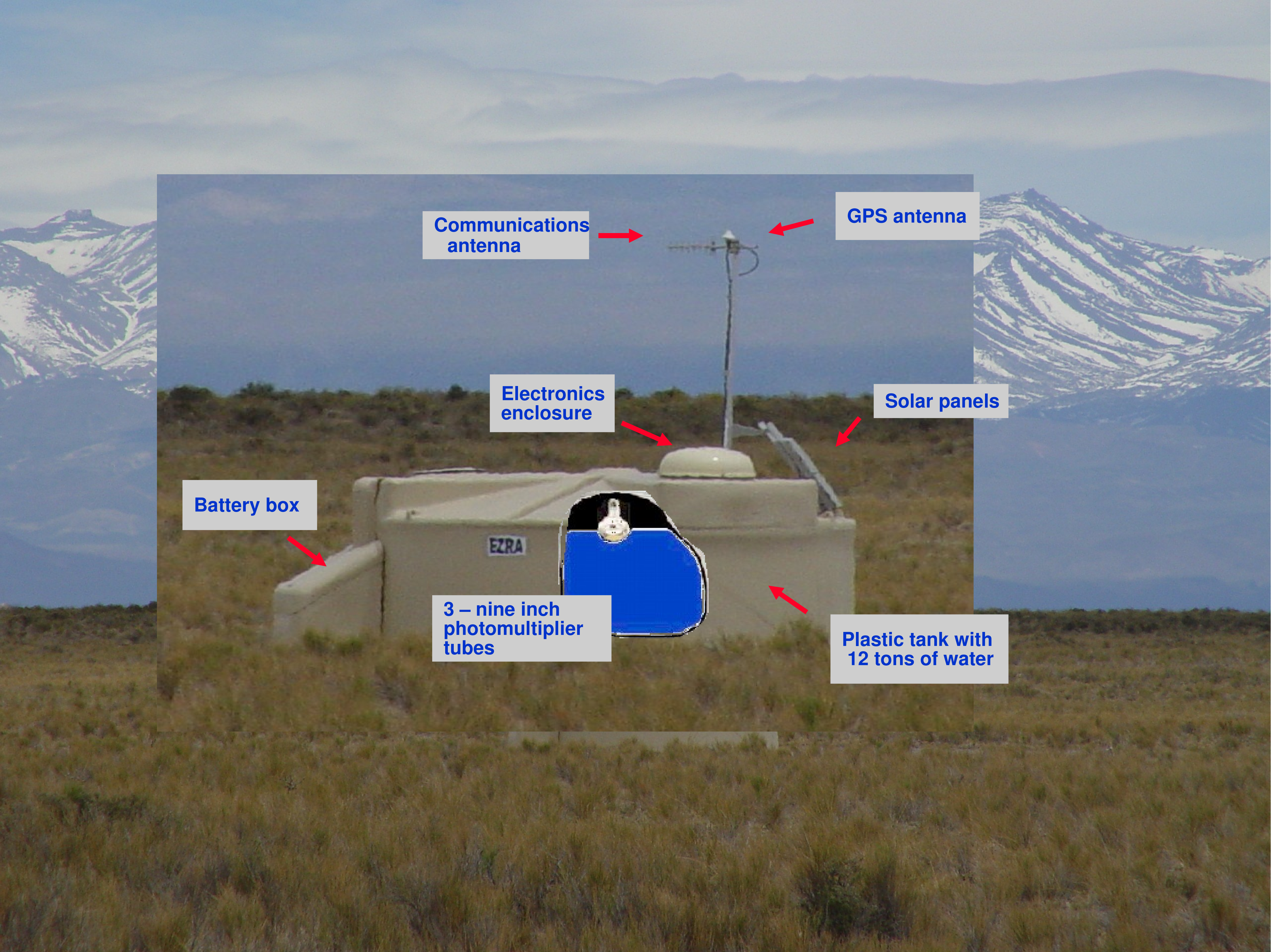
Communications antenna
GPS antenna
Electronics enclosure
Solar panels
Battery box
EZRA
3 – nine inch photomultiplier tubes
Plastic tank with 12 tons of water



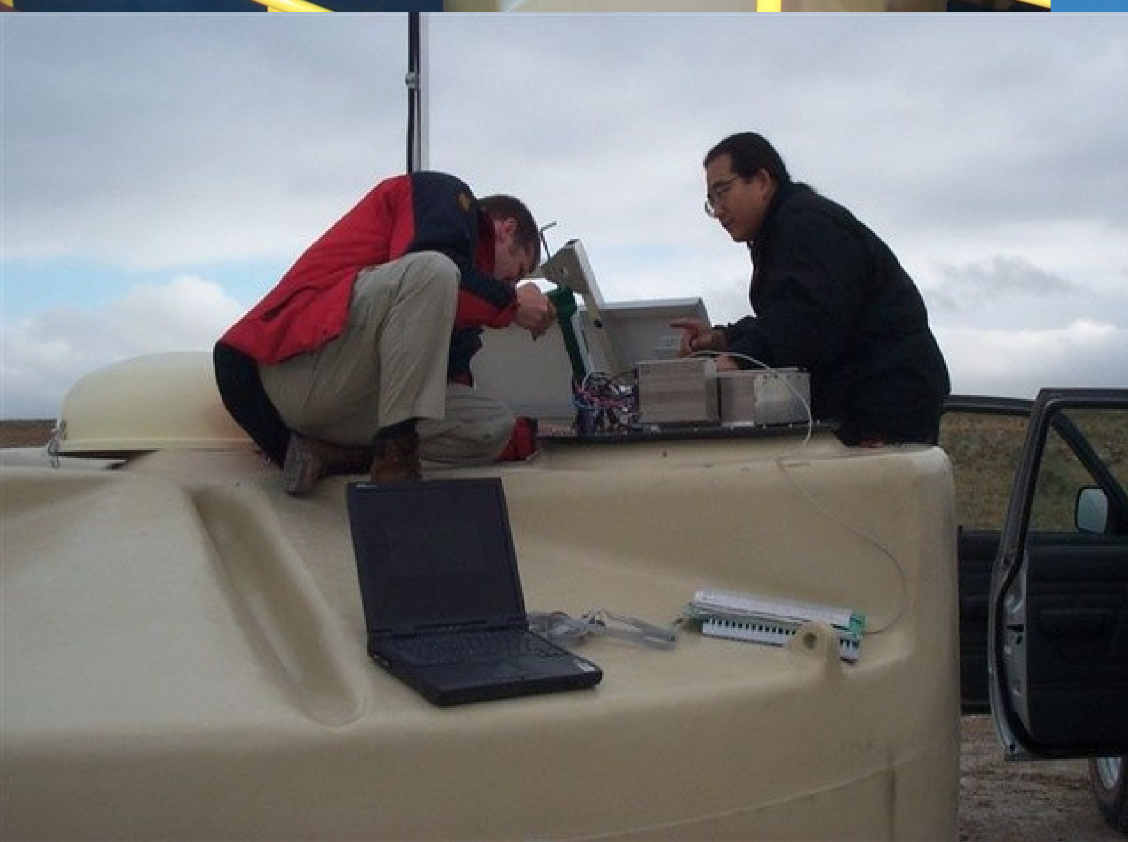


Surface Detector Event

Θ~ 60º, ~ 86 EeV

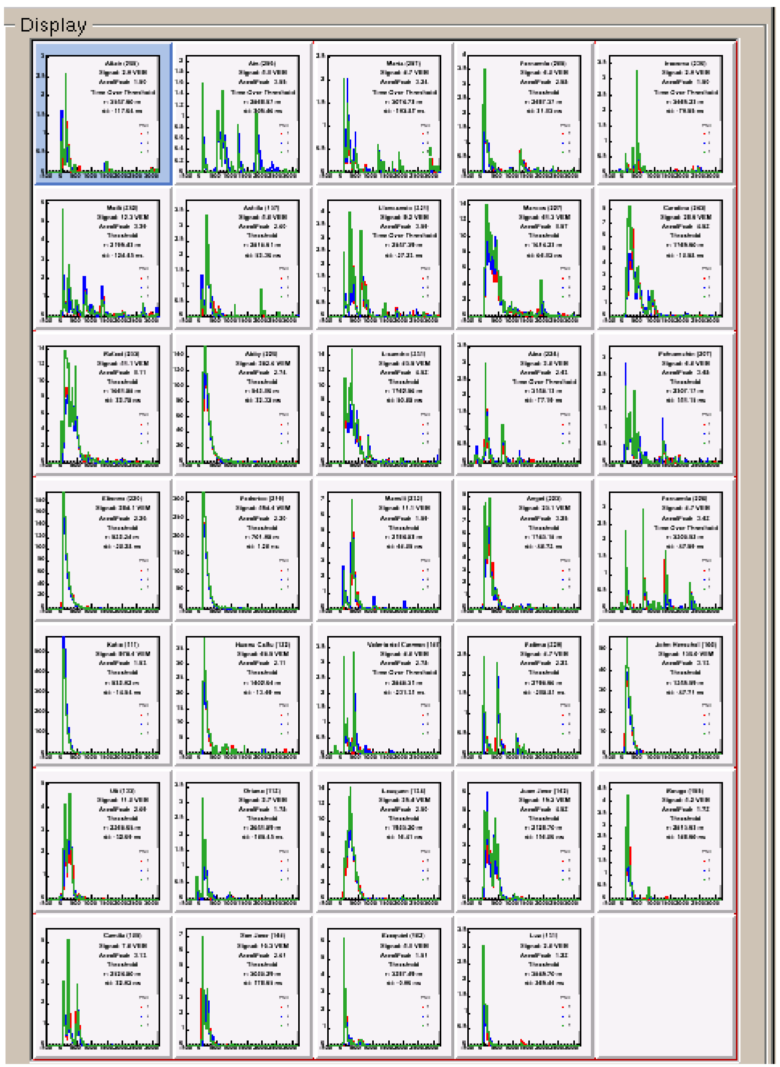

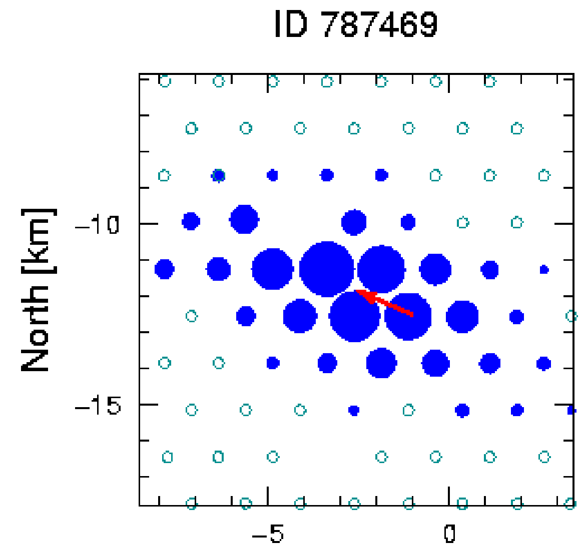

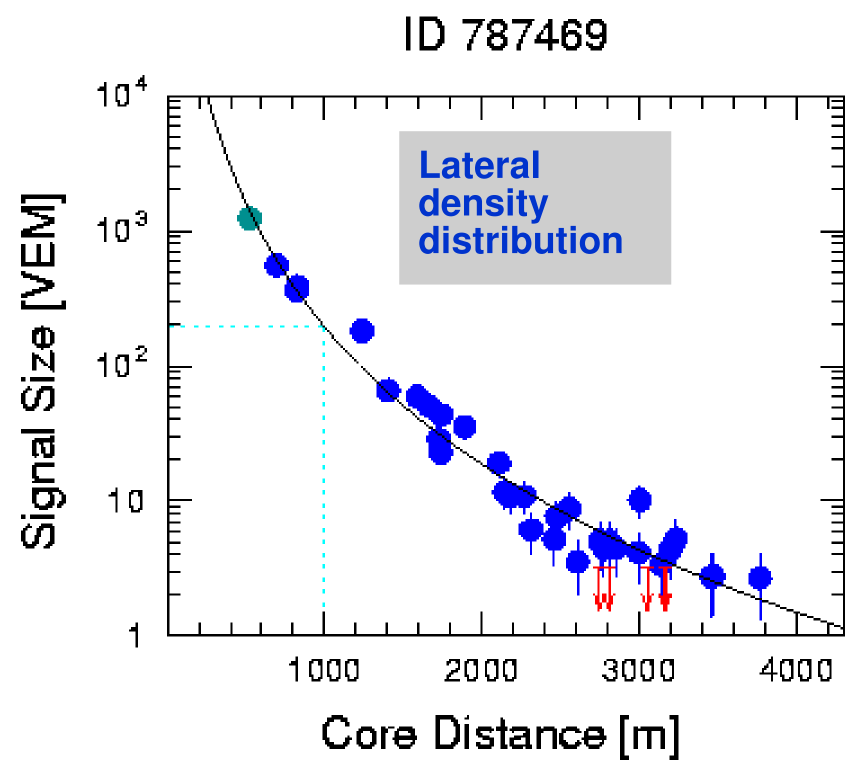

The energy converter:

Compare ground parameter S(1000) with the fluorescence detector energy.

Transfer the energy converter to the surface array only events.

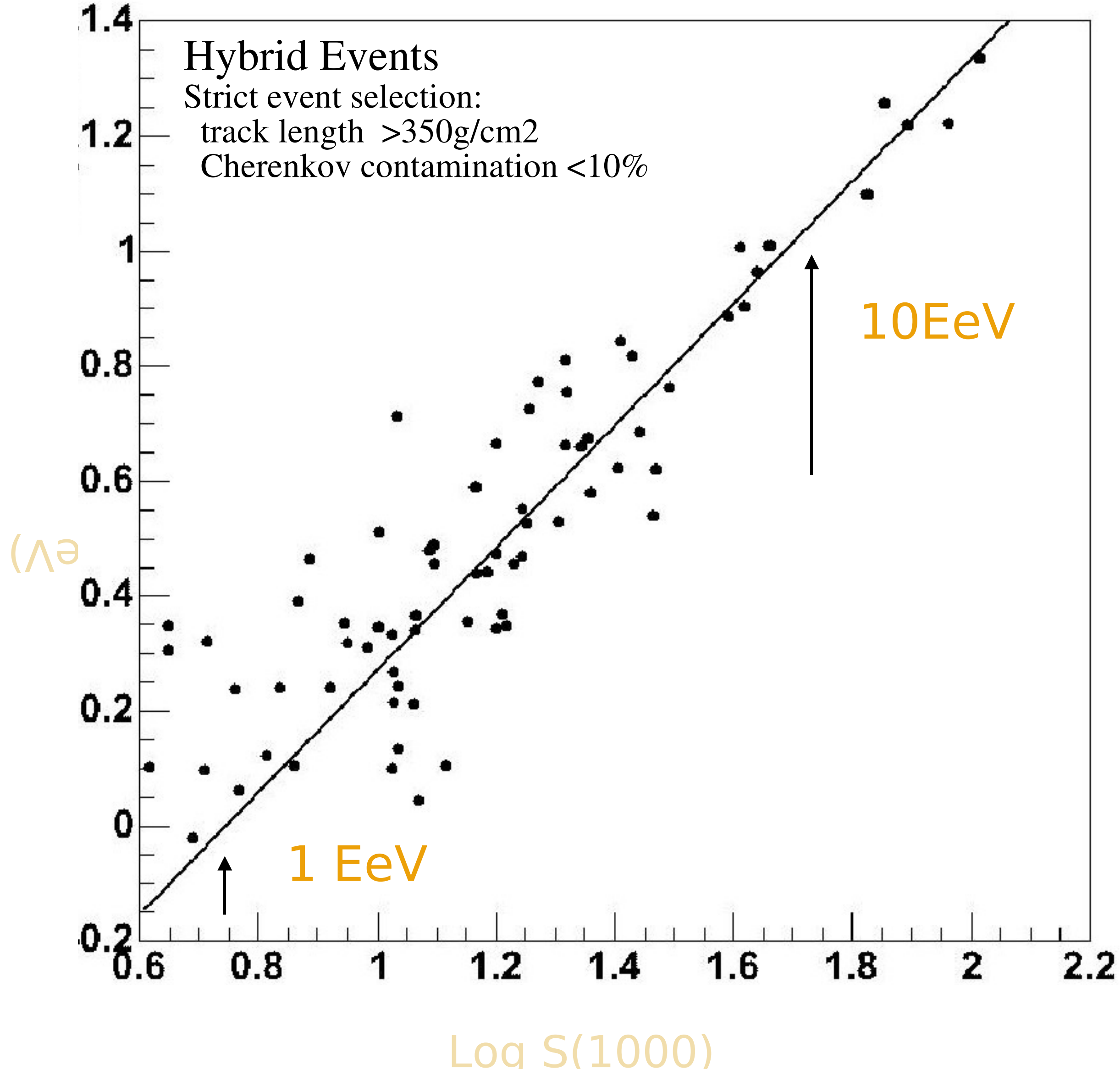

Physics of Fluorescence Detectors

Charged particles from EAS interact with Nitrogen Molecules . The Nitrogen Molecules get excited and they emit later (when returning to their ground state) a typical radiation in the wave length range between 300 nm to 400 nm.

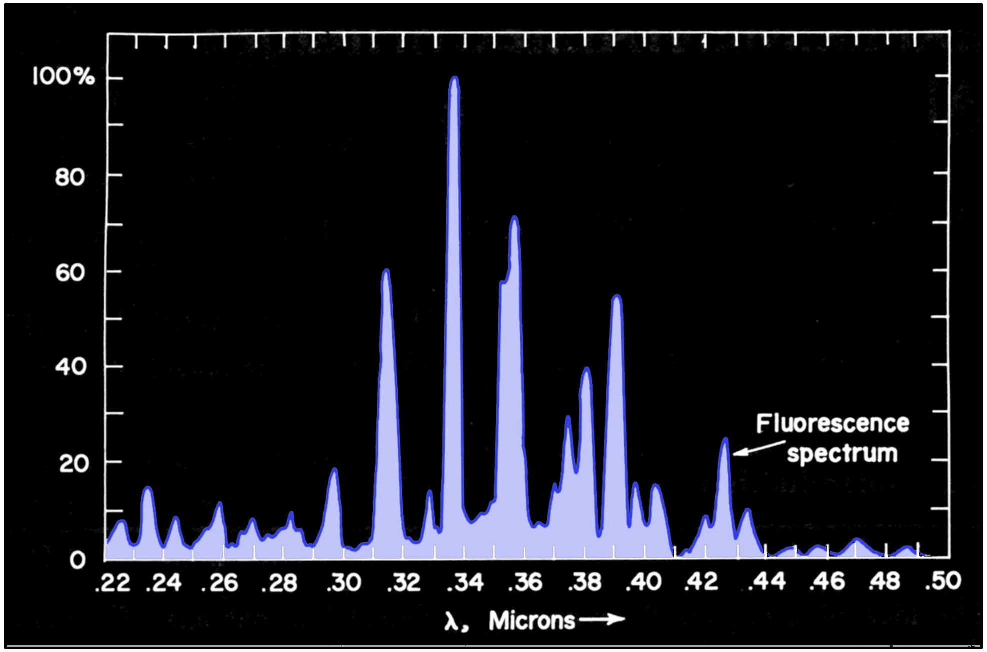

Fluorescence Spectrum

fluorescence yield
between 300 - 400nm

approx. 4 photons per shower particle per metre of track

This radiation (commonly called fluorescence light) can travel several kilometers throught the atmosphere (without being absorbed or scattered), and detected by an optical telescope with fast response electronics (fluorescence detectors).

Basic Description of a Fluorescence Detector

The fluorescence light is collected by a mirror or a lens and imaged on to a camera that contains PMTs.

Each PMT receives light coming from a specific region of the sky.

When an EAS crosses the field of view of a fluorescence detector, It triggers some of the PMTs.

Each triggered PMT records the trigger time and the intensity of the signal and together with the PMT's observing direction are used to determine the arrival direction, the shower longitudinal profile (Xmax) and the energy of the primary CR.

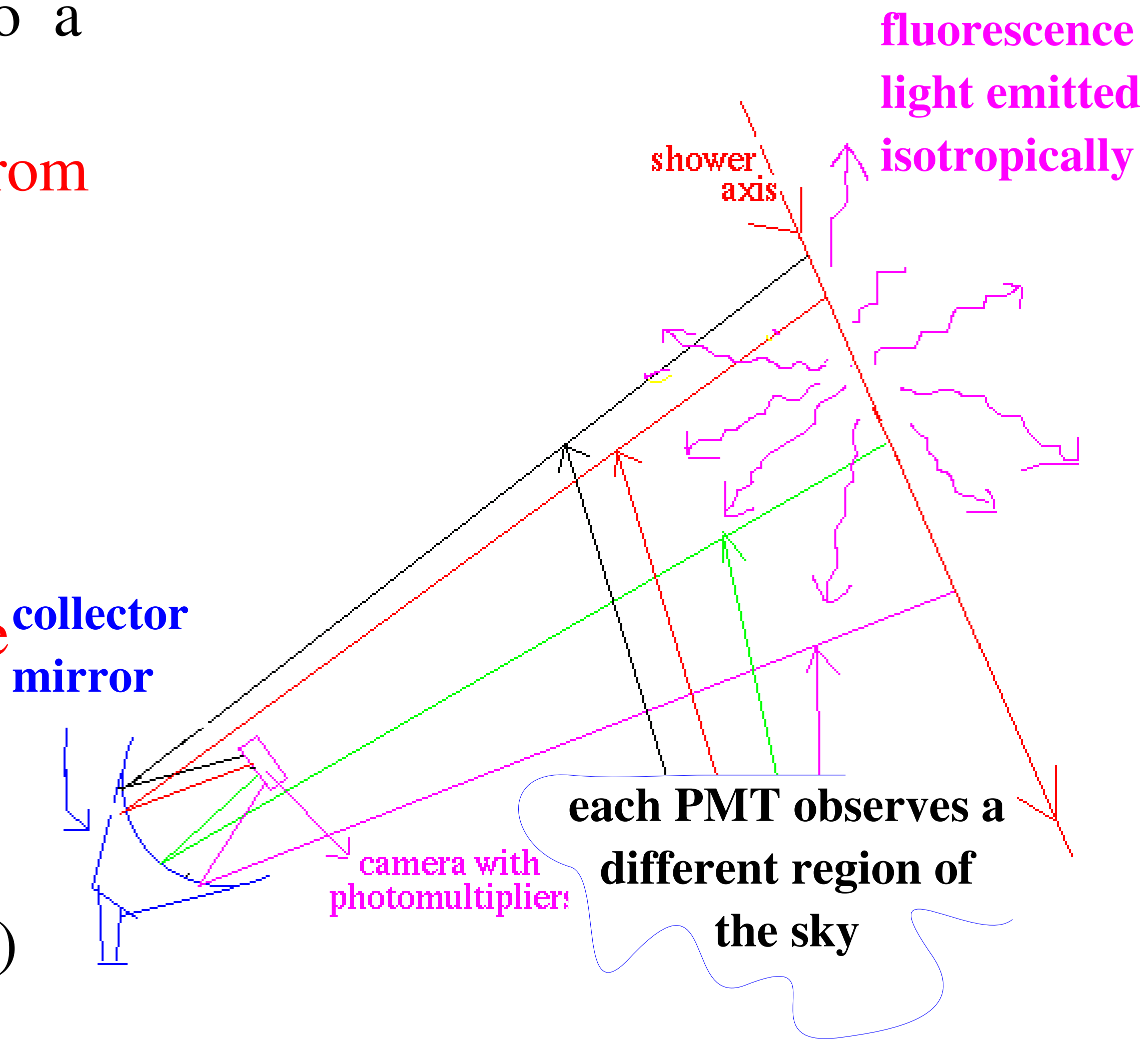

Evolution of the Fluorescence Detectors

The First Fly's Eye - New York 1967

Sky & Telescope October 1967

Greisen, Bunner et al.

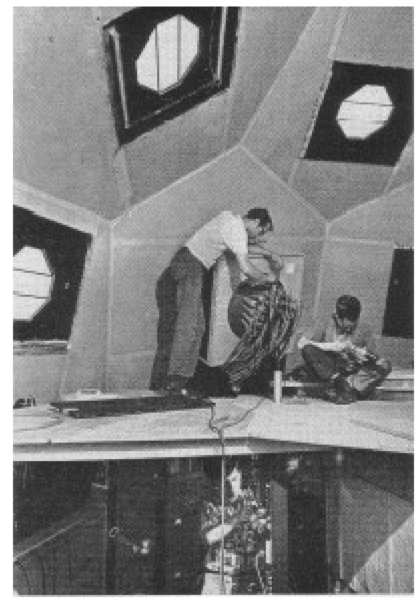

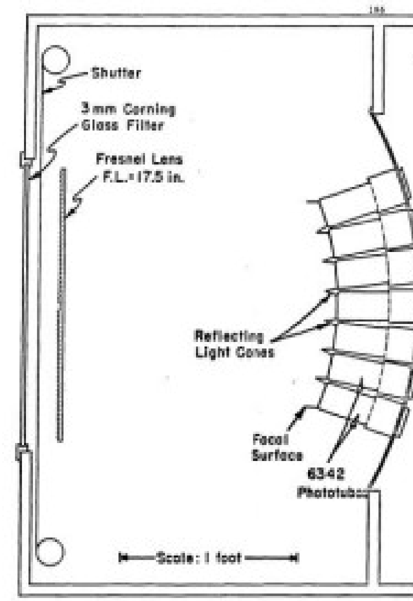

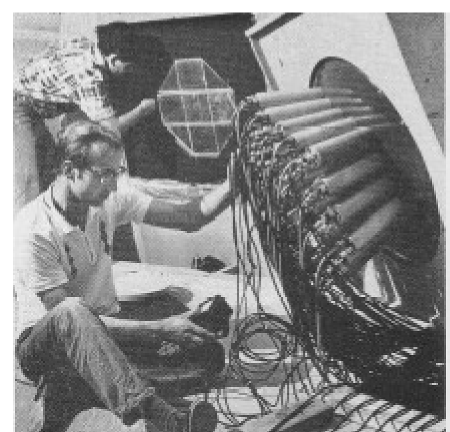

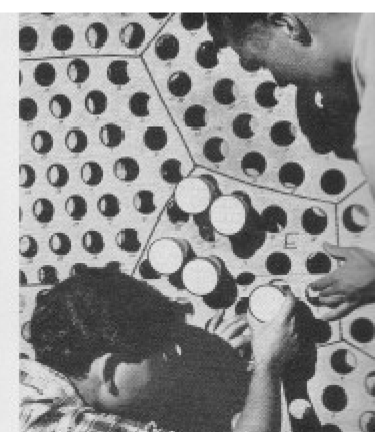

Evolution of the Fluorescence Detectors

VOLUME 39, NUMBER 13 PHYSICAL REVIEW LETTERS 26 SEPTEMBER 1977

Measurement of Light Emission from Remote Cosmic-Ray Air Showers

H. E. Bergeson, G. L. Cassiday, T.-W. Chiu, D. A. Cooper, J. W. Elbert, E. C. Loh, D. Steck, and W. J. West
Department of Physics, University of Utah, Salt Lake City, Utah 84112

and

J. Linsley
Department of Physics and Astronomy, University of New Mexico, Albuquerque, New Mexico 87131

and

G. W. Mason
Department of Physics and Astronomy, Brigham Young University, Provo, Utah 84602

(Received 28 June 1977)

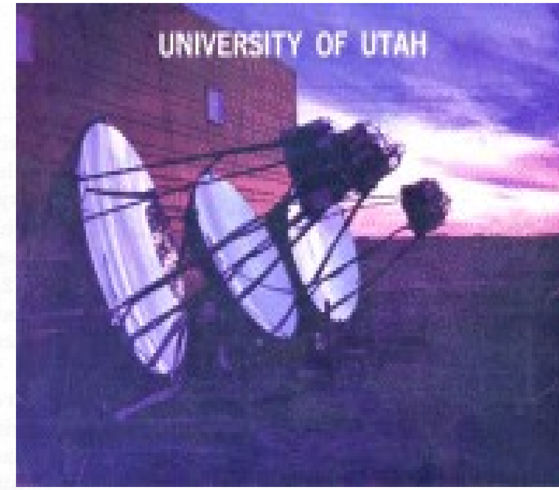

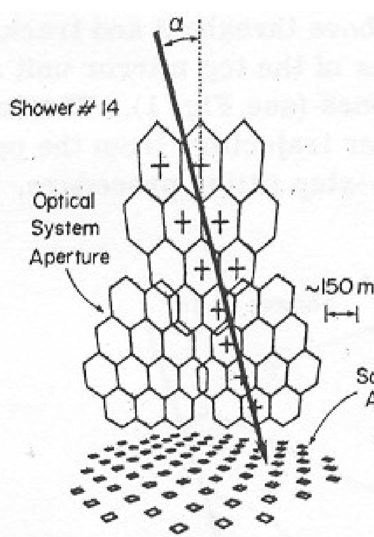

FIG. 1. Projection of the aperture of the optical detector onto a vertical plane above the center of the Volcano Ranch scintillator array. A reconstructed shower trajectory is indicated by the heavy line. Crosses denote phototube apertures in which a signal was detected.

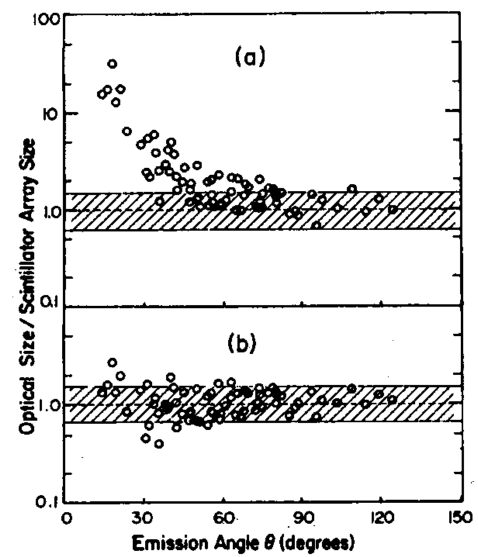

FIG. 4. Ratios of sizes obtained from the optical data to sizes measured by the Volcano Ranch array using (a) computed scintillation light only and (b) estimated light from all sources. Data are plotted for each phototube in all fifteen reconstructed showers. The shaded bands display the uncertainty due to systematic effects in both size measurements.

Utah Fly's Eye 1981-1993

Cassiday, Bergeson, Loh, Sokolsky et al.

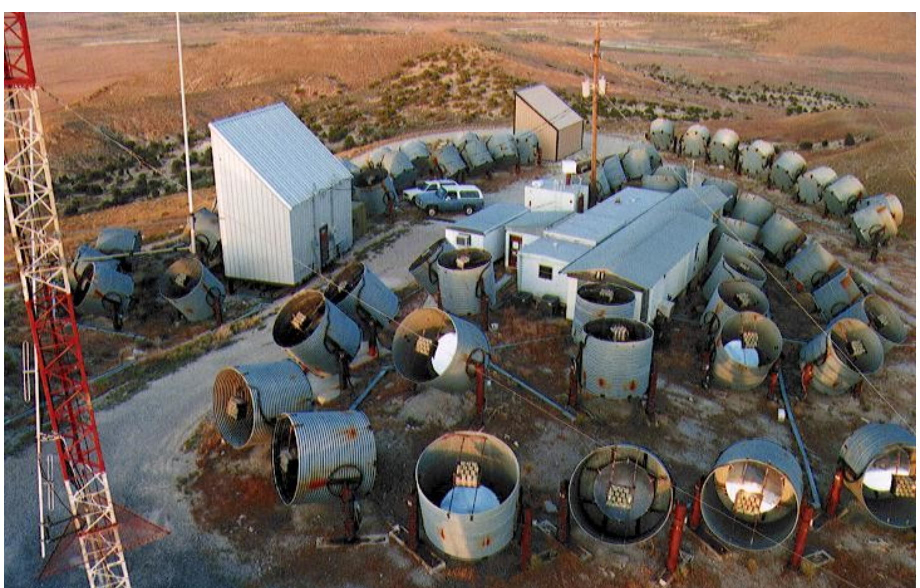

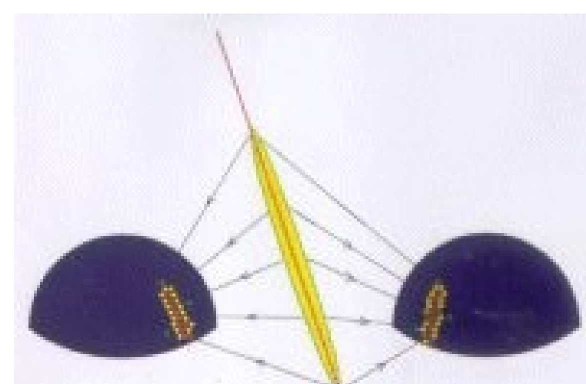

Evolution of the Fluorescence Detectors

High Resolution Fly's Eye

(1997 -2005)

One of two sites 13km apart - Dugway, western Utah
Collecting area in excess of $3000 km^2$ at highest energies

Evolution of the Fluorescence Detectors

The Fluorescence Detector from the Pierre Auger Experiment

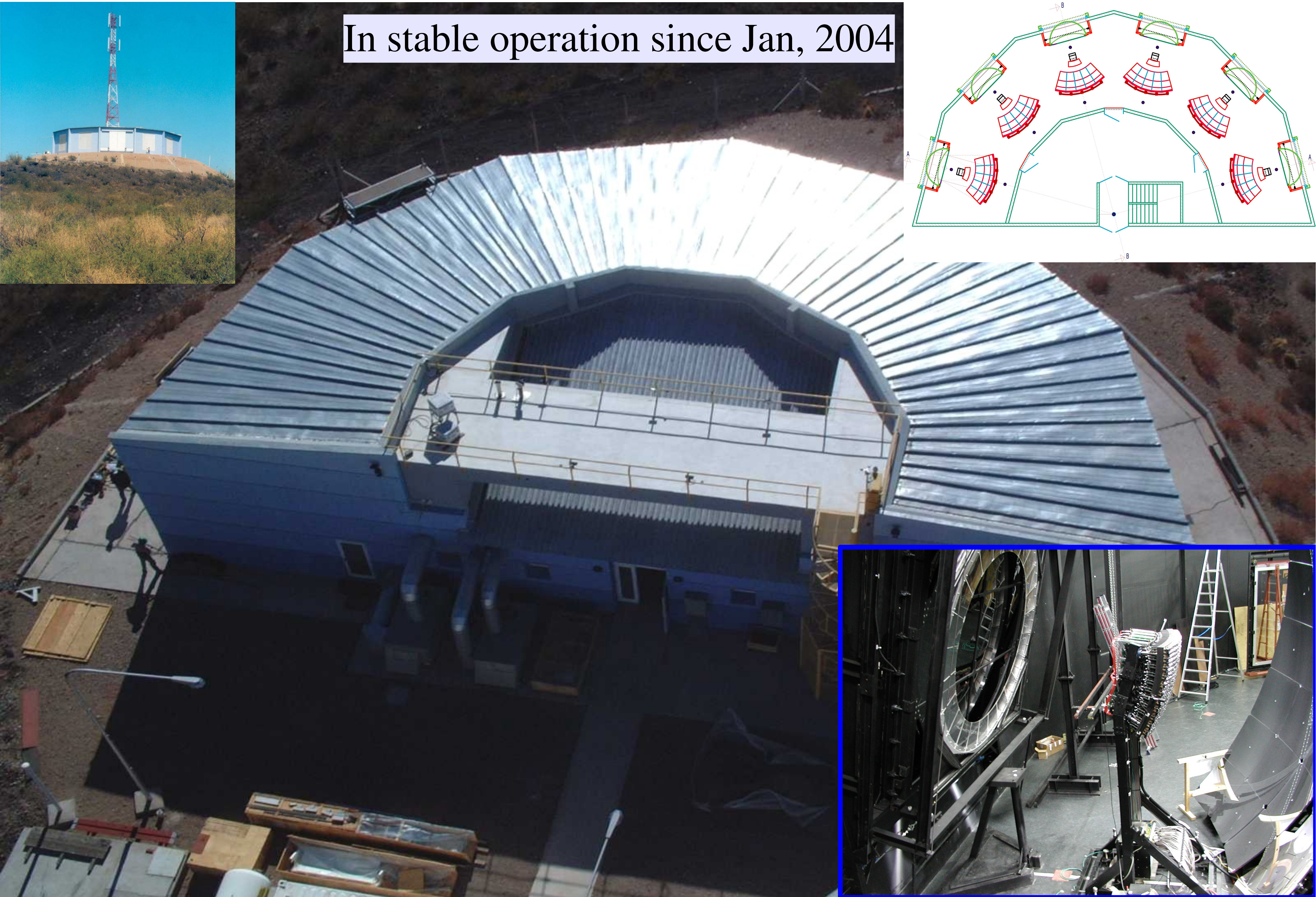

In stable operation since Jan, 2004

Evolution of the Fluorescence Detectors

EUSO, A Fluorescence Telescope on Space

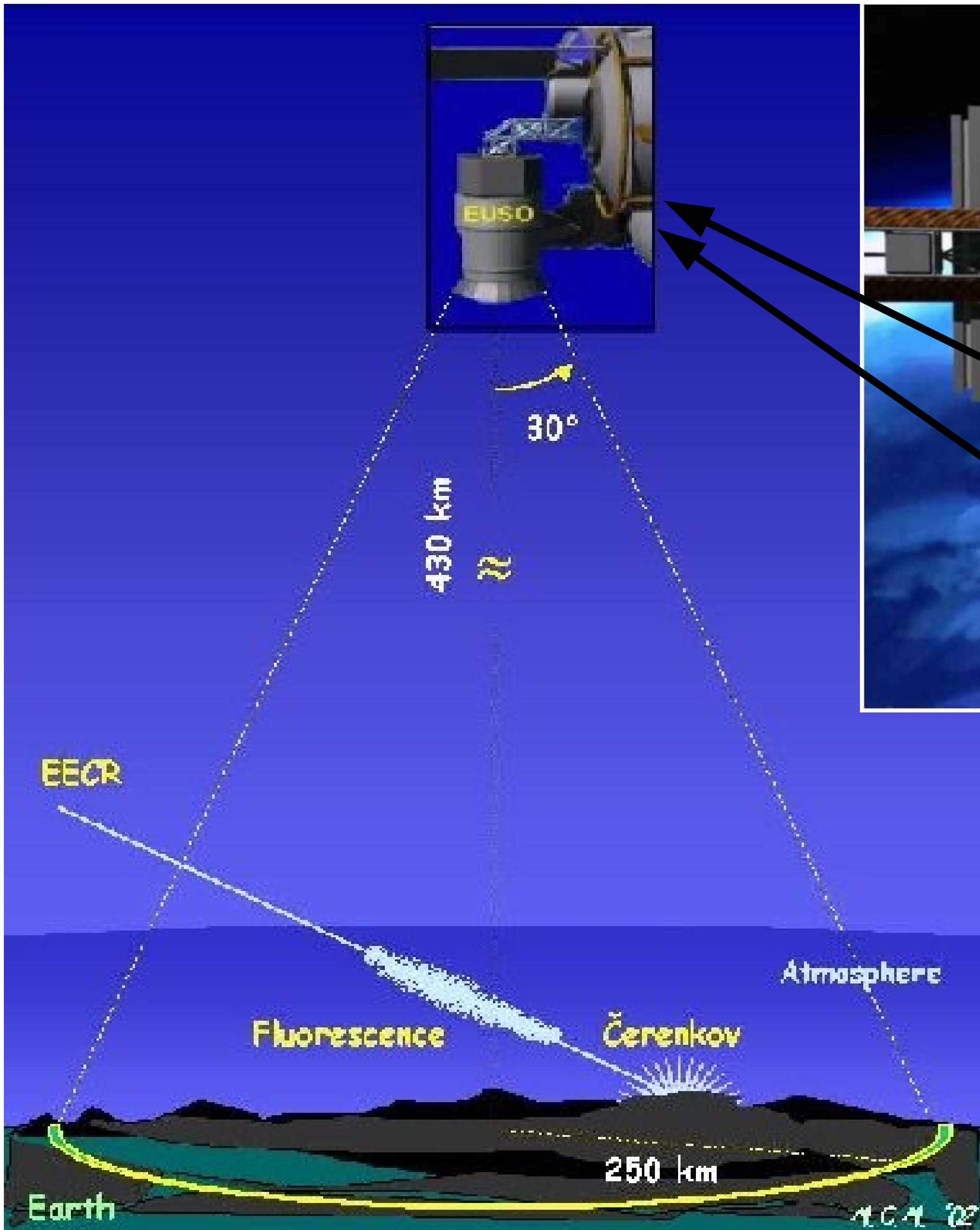

Currently under "Phase A", with a goal for a three years mission starting in 2010

Reconstructing Air Showers with Fluorescence Detectors

Recovering:

the arrival direction,
the primary energy and
the composition

From:

-PMT's observing direction
-PMTS' triggering time
-PMT's recorded signal.

Reconstructing The CR Arrival Direction

The arrival direction is obtained in two separate steps:

1. The observing directions of the triggered pixels and the detector itself define a plane that is called Shower Detector Plane (SDP).

2.- The SDP contains the EAS axis. The orientation of the shower axis within the SDP is obtained using the trigger times from the PMTs.

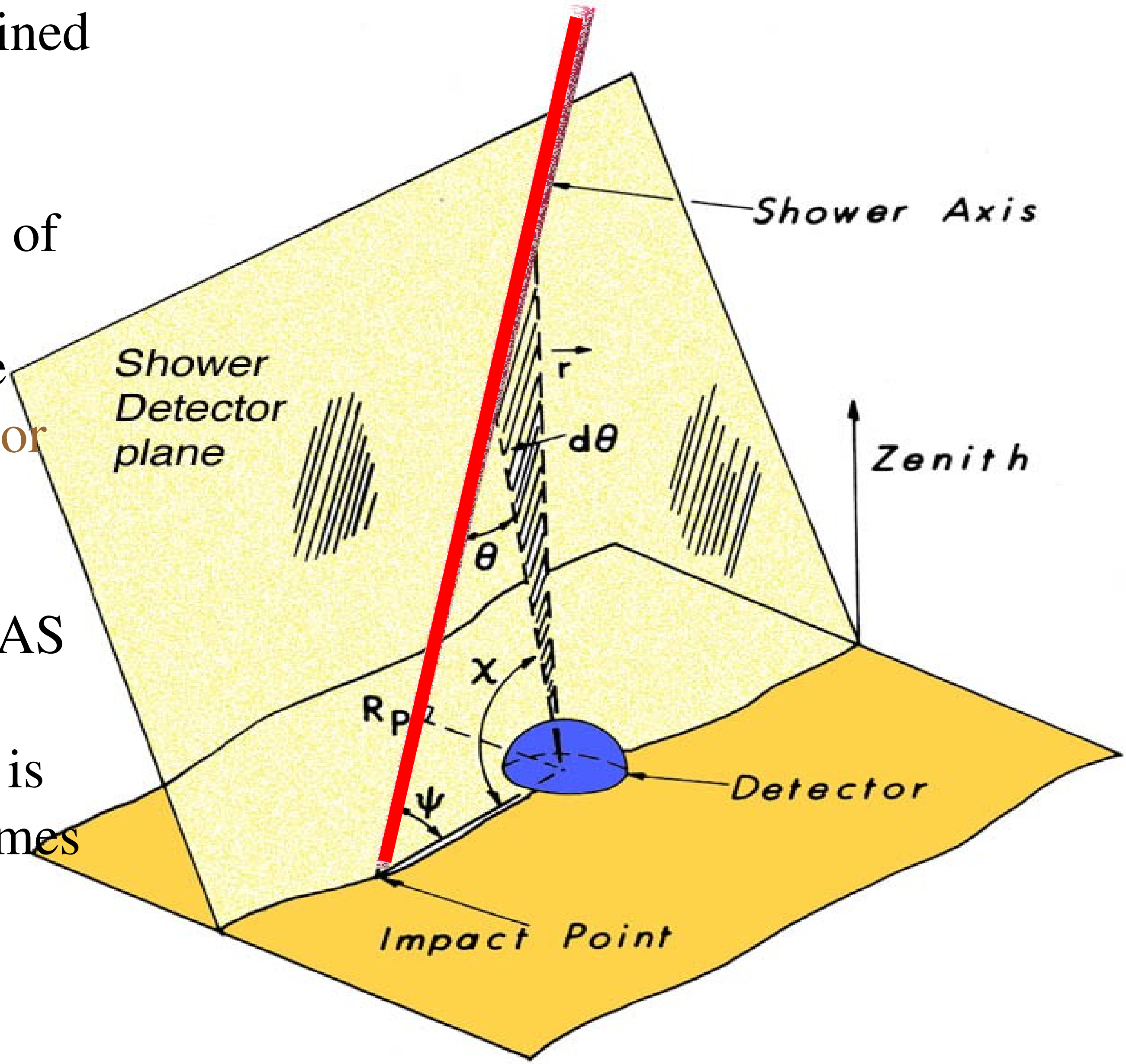

Reconstructing The CR Arrival Direction

Step 1: Reconstructing the SDP

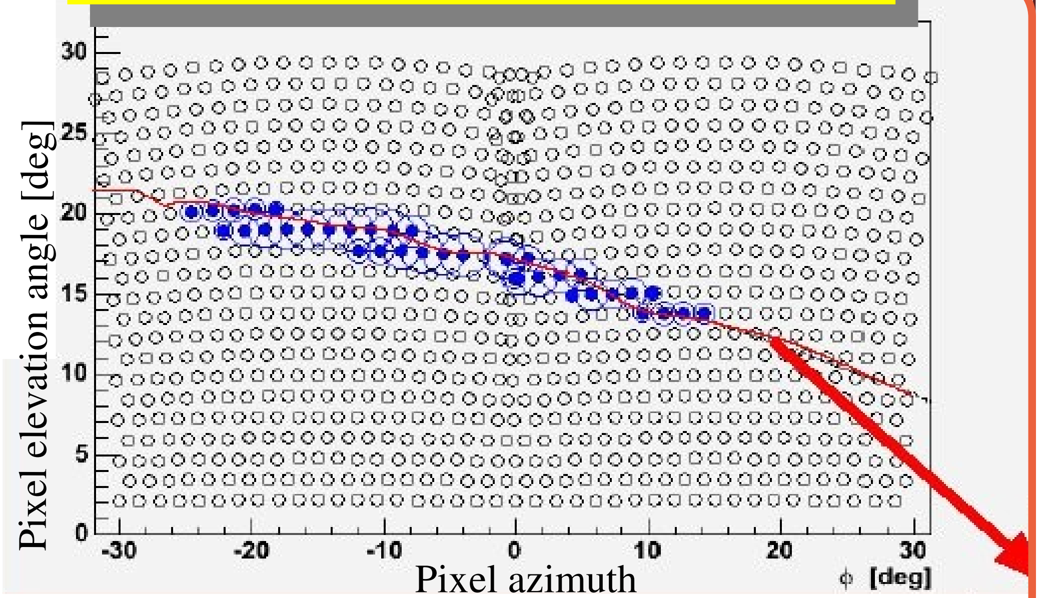

Step 2: Reconstructing the Shower axis

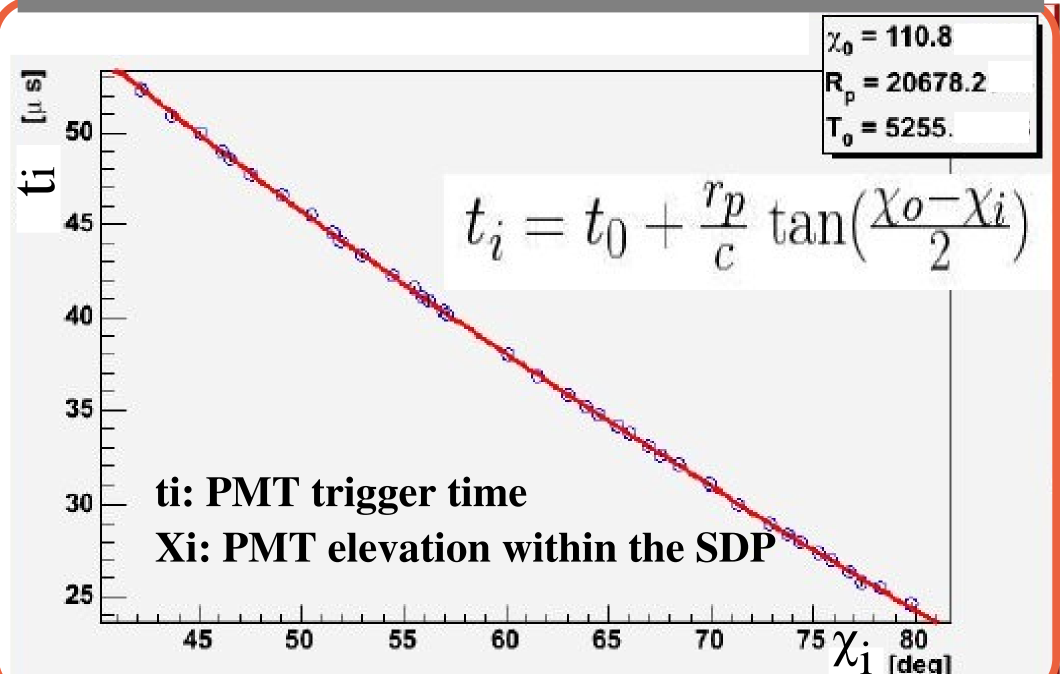

$$t_i = t_0 + \frac{r_p}{c}\tan\left(\frac{\chi_o - \chi_i}{2}\right)$$

ti: PMT trigger time

Xi: PMT elevation within the SDP

The parameters that define the shower geometry are:

Rp: Closest distance to the axis.

Xo: Angle between the axis and the horizontal plane.

to: Time when the shower front crosses the Rp point.

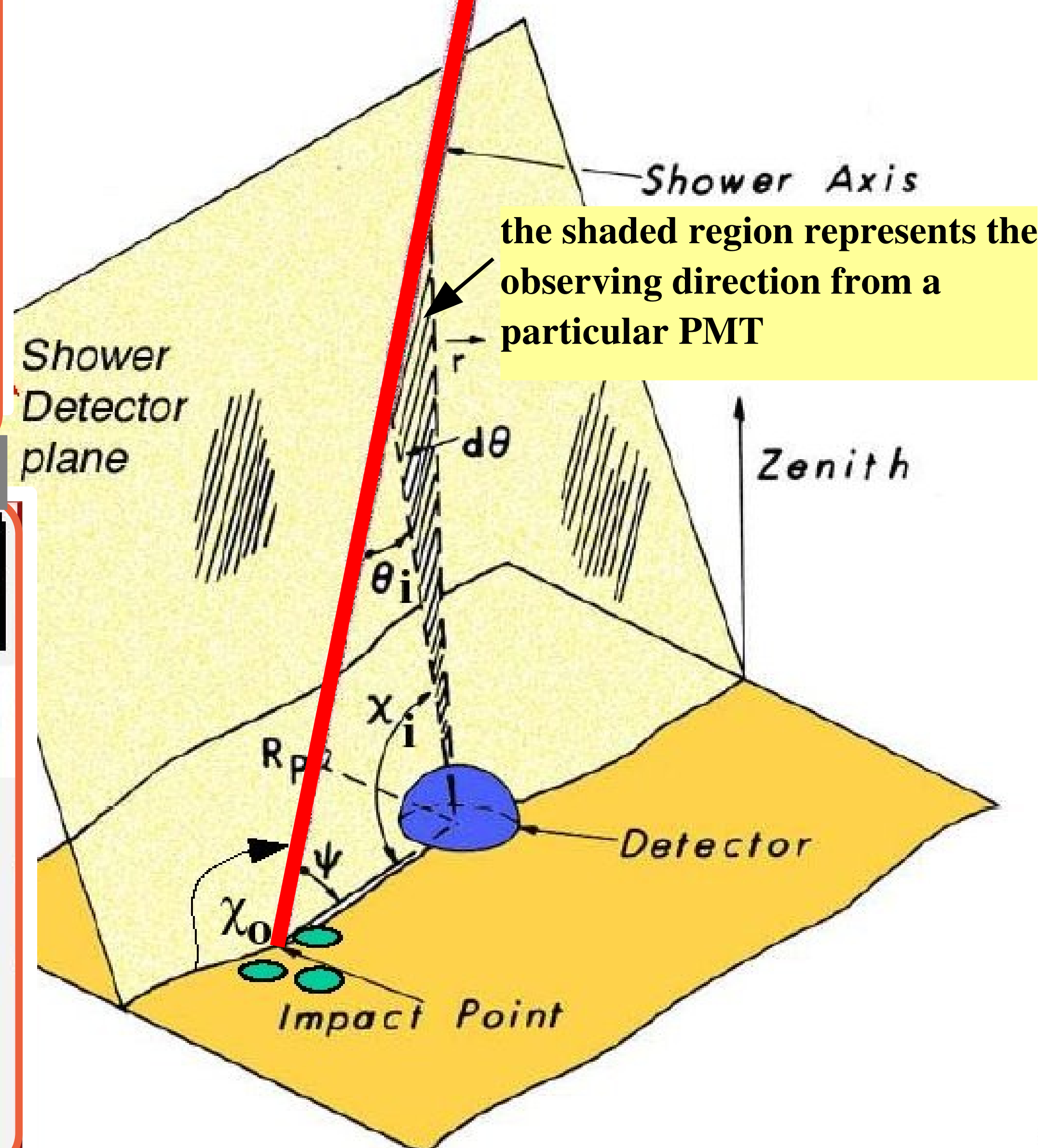

Reconstructing The CR Arrival Direction

The parameters that define the shower geometry are:

Rp: Closest distance to the axis.

Xo: Angle between the axis and the horizontal plane.

to: Time when the shower front crosses the Rp point.

Step 1: Reconstructing the SDP

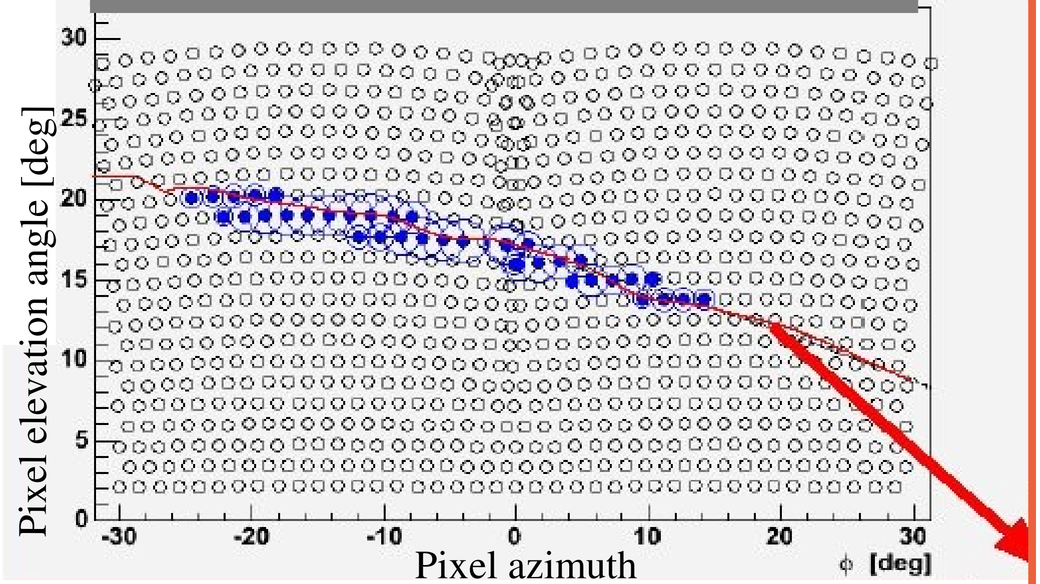

Step 2: Reconstructing the Shower axis

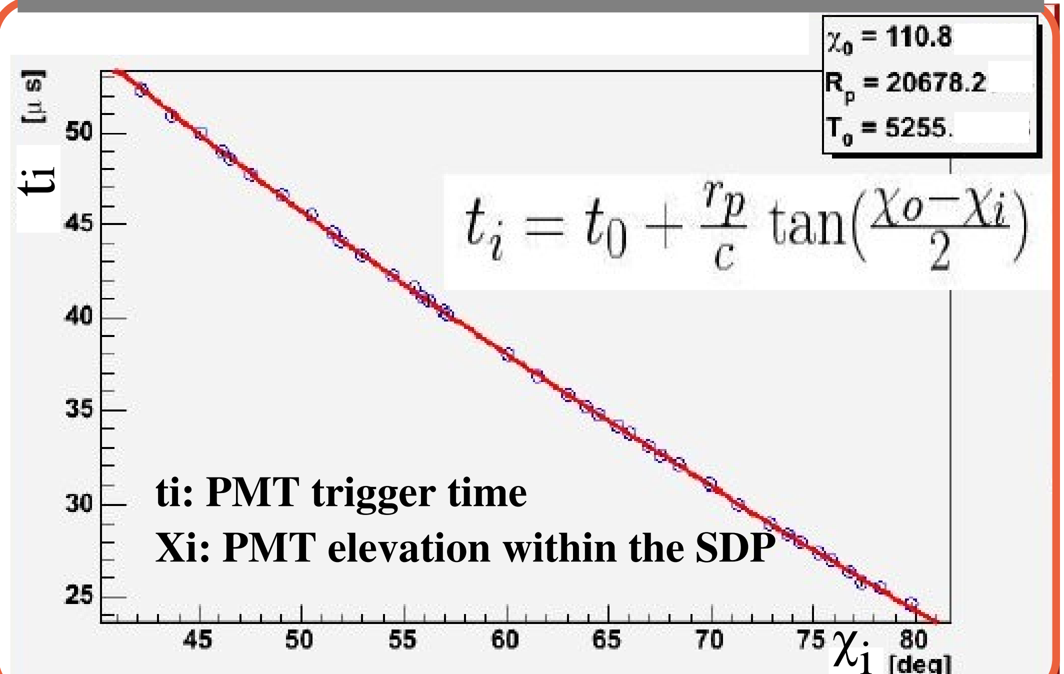

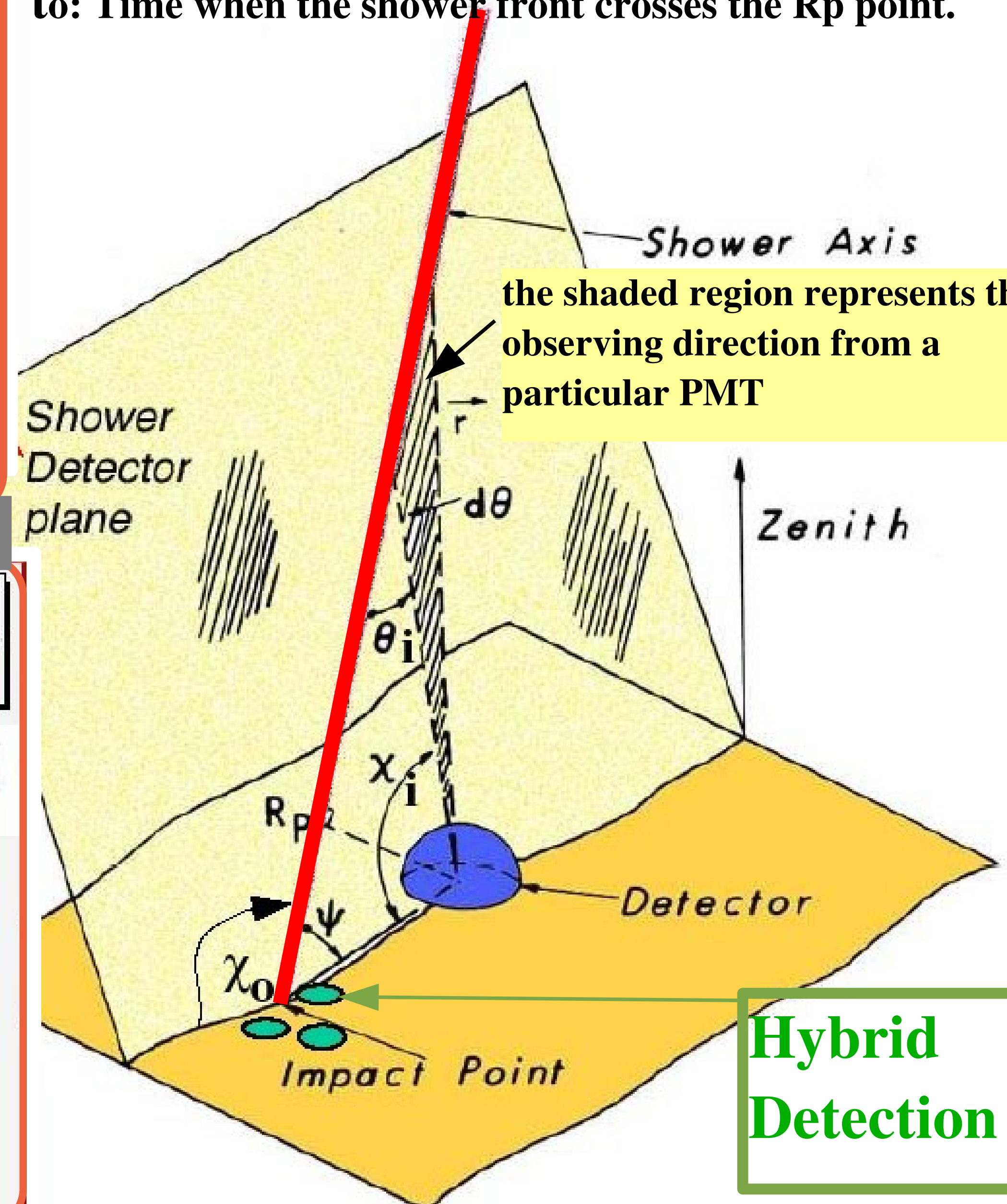

Hybrid Detection

Reconstructing The CR Arrival Direction

Typical stereo HiRes event

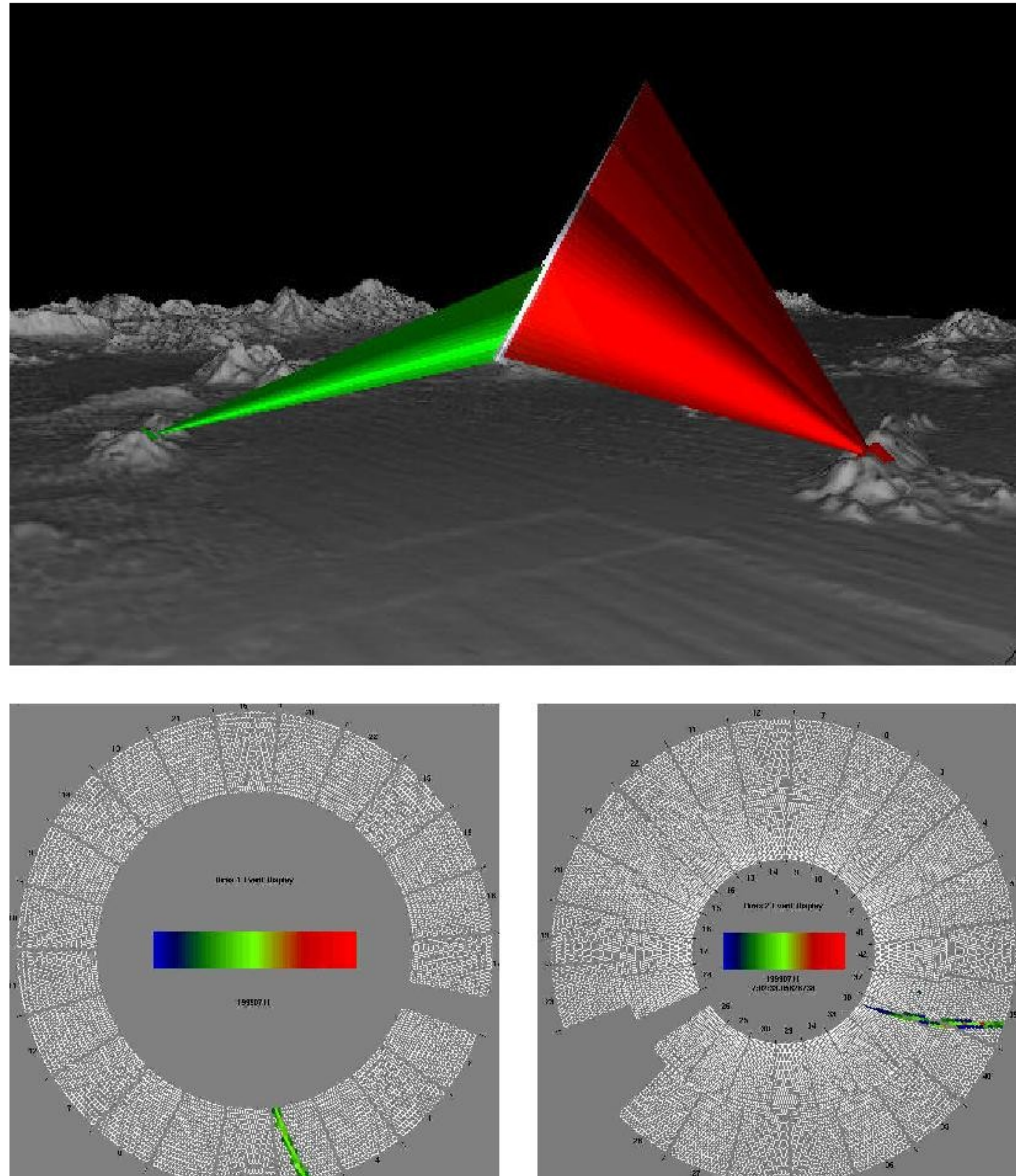

When an EAS is observed by two or more FDs the arrival direction is defined by the intersection of the SDPs.

Stereo events provide some advantages:

- better geometry resolution
- the shower profile is observed by two eyes.
- checks of systematics

Reconstructing The CR Energy

(Preliminary Concepts)

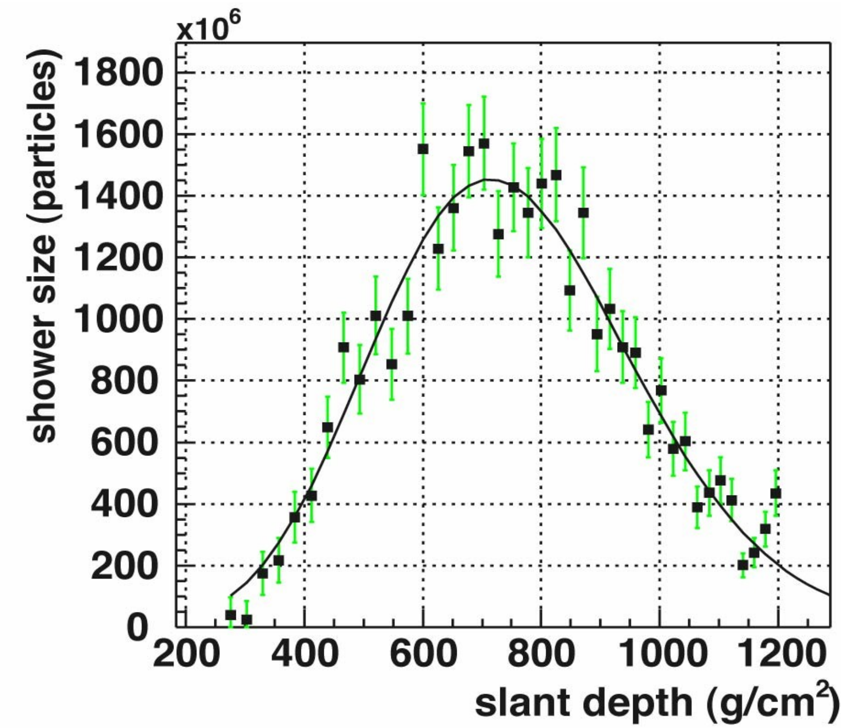

The shower profile has a shape that can be parametrized by:

The Gaisser-Hillas Function

$$N_e(X) = N_{max}\left(\frac{X-X_0}{X_{max}-X_0}\right)^{\frac{(X_{max}-X0)}{\lambda}} e^{\frac{X_{max}-X}{\lambda}}$$

where:

Ne: The number of electrons (shower size)

Xmax: Depth of shower maximum

Nmax: Shower size at Xmax

λ , χo: shape parameters

Slant depth or atmospheric depth $= \int \rho(l)_{atmosphere}\, \mathrm{d}l$

Reconstructing The CR Energy

Generation of Cerenkov Light

The energetic electrons apart from generating fluorescence light, They generate a flux of **Cerenkov light**.

The **Cerenkov light** is emitted almost parallel to the shower axis, within ~ 25° of the shower axis..

Depending on the shower geometry, some **Cerenkov light** can reach directly the detector, or be scattered towards the detector.

The **Cerenkov light** represents part of the background light for the fluorescence signal.

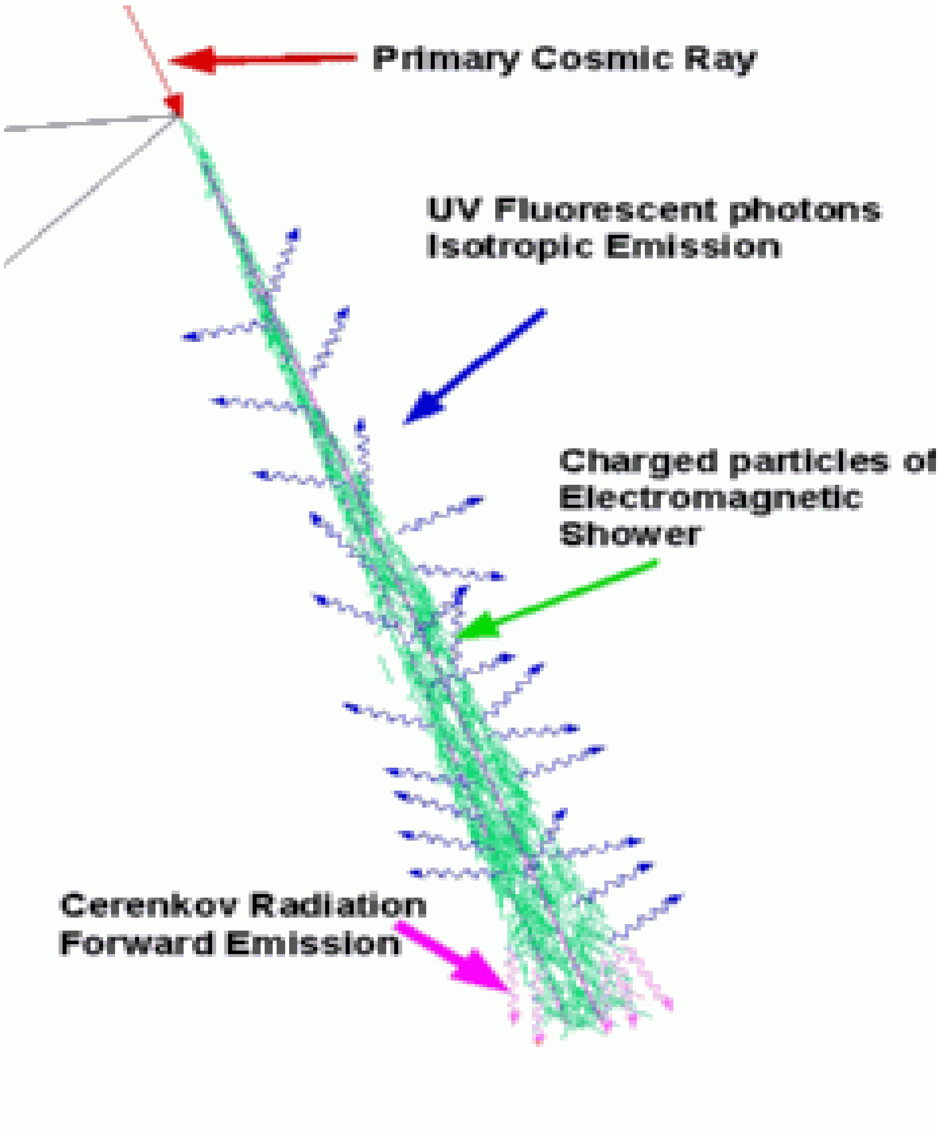

Propagation of light trough the atmosphere

Light propagating trough the atmosphere may suffer

Rayleigh or Mie Scattering

Reconstructing The CR Energy

. . . Propagation of light trough the atmosphere

Rayleigh scattering: Rayleigh scattering is an electromagnetic process well understood and can be easily calculated since it only depends on the atmospheric density (ρ) and the photon's wave length (λ). The number of photons scattered out of the beam per unit length can be written as:

$$\frac{dN_\gamma}{dl} = -\frac{\rho N_\gamma}{X_R}\left(\frac{400nm}{\lambda}\right)^4$$

where N_γ is the number of photons in the beam, and X_R is the mean free path for scattering (X_R at $\lambda = 400$ nm is 2970 g/cm^2).

and the Rayleigh angular distribution is given by:

$$\frac{d^2N_\gamma}{dl\,d\Omega} = \frac{3}{16\pi}\left|\frac{dN_\gamma}{dl}\right|(1+cos^2\theta)$$

θ is the scattered angle

Reconstructing The CR Energy

Transmission factor for Rayleigh scattering

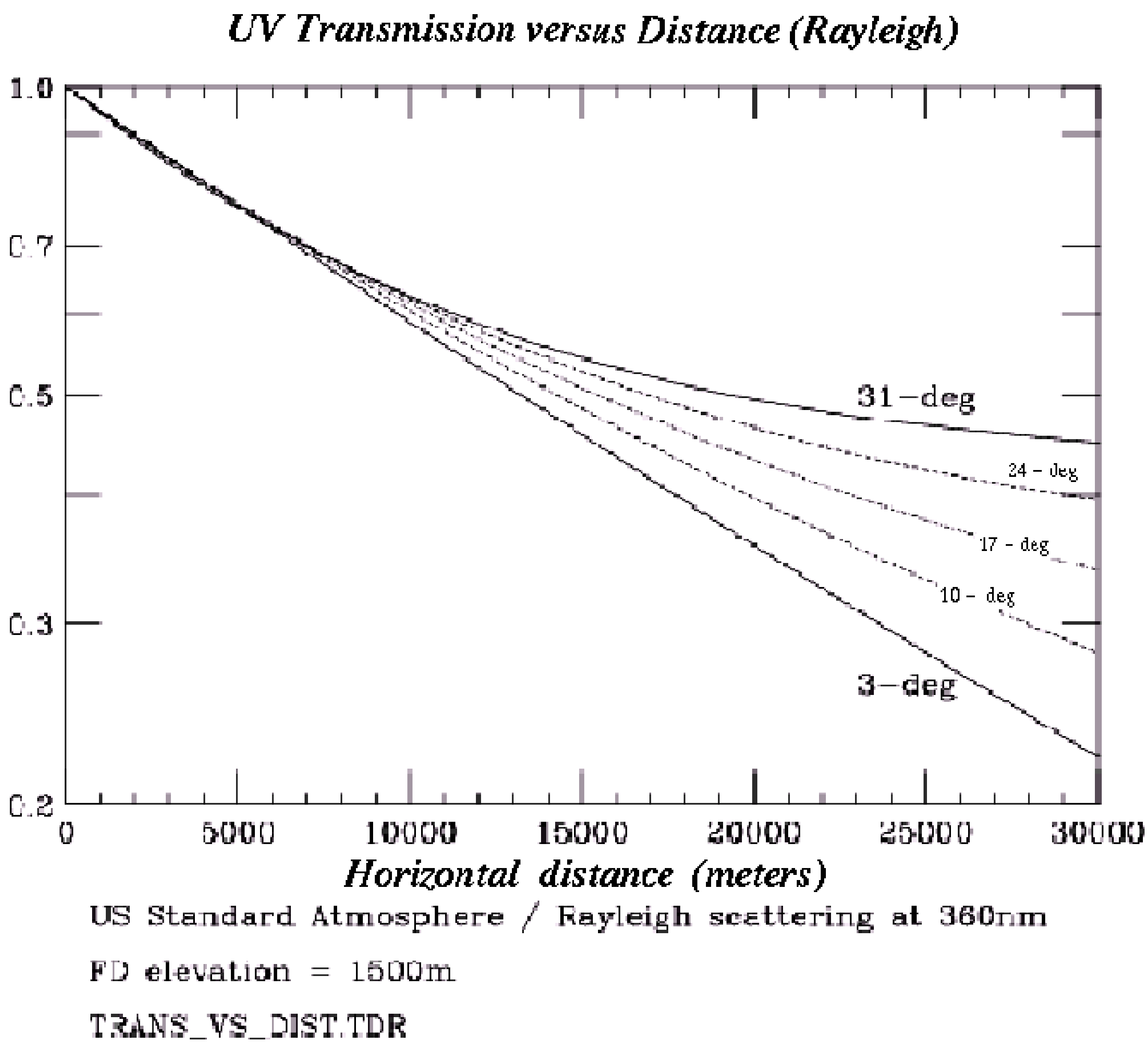

Propagation of light trough the atmosphere

Mie scattering: The Mie scattering or aerosol scattering is not easy to calculate, since it varies with the aerosol shape, aerosol size and aerosol dielectric constant. In addition, the aerosol contents are variable in the atmosphere. The aerosols may change as a function of altitude, composition of pollutants, and weather conditions.

The Mie angular distribution depends on wavelength and aerosols characteristics. However it is strongly peaked in the direction of the photon. Therefore, Mie scattering will dominate over Rayleigh scattering at small scattering angles.

Mie Scattering

Mie transmission factor (for the UV range) as a function of the horizontal distance for tube elevation angles from 3°to 31°.

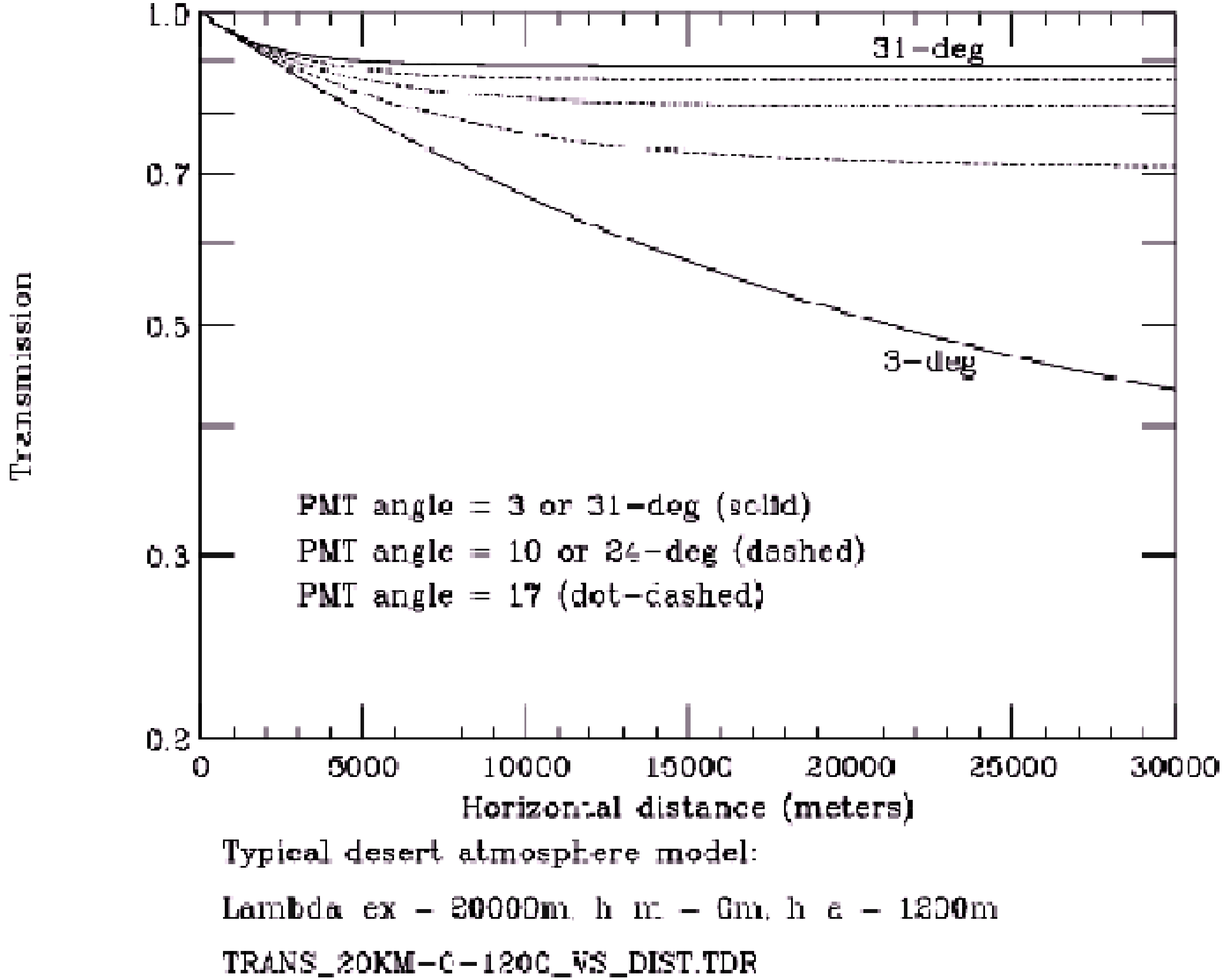

Reconstructing The CR Energy

Mie Scattering

To avoid the higher levels of aerosol concentrations in the atmosphere, the fluorescence detector should be located at the top of some mountains.

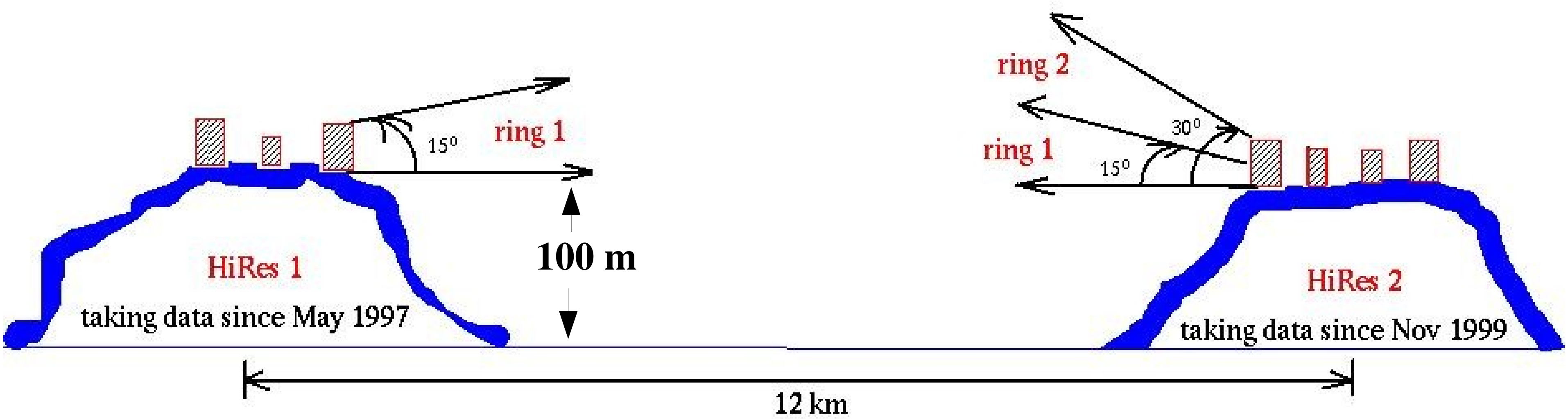

Schematic representation of the HiRes detector

Fluorescence Yield Measurements

The Fluorescence Yield has been measured in the lab by several experiments

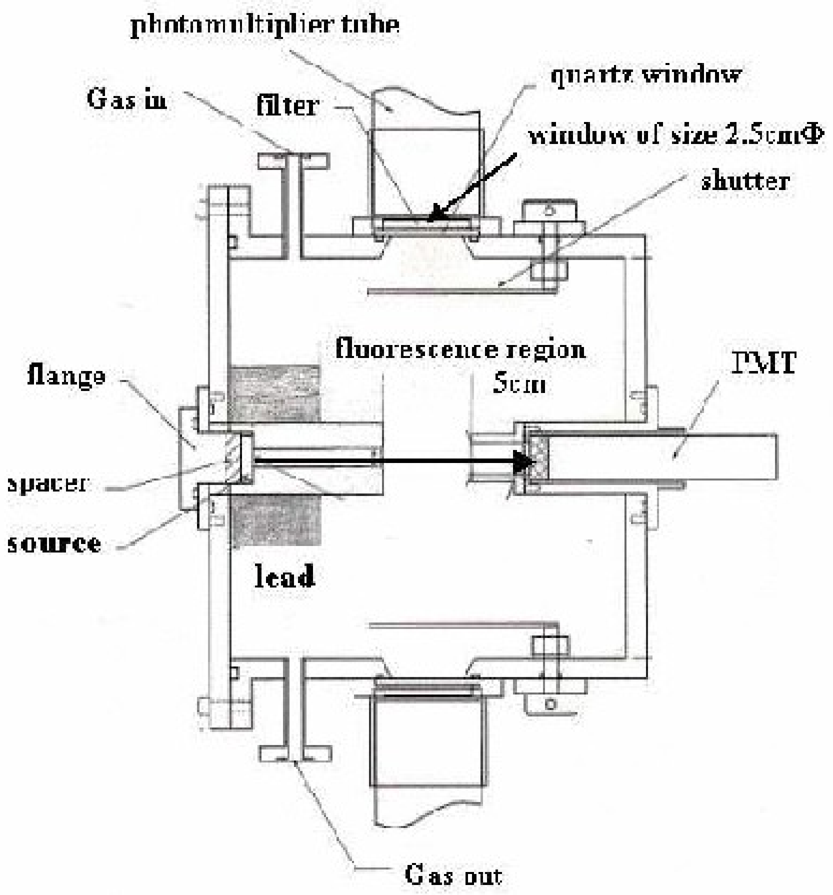

Nagano et al. Astroparticle Phys. 20 (2003) 293

Reconstructing The CR Energy

Fluorescence Yield Vs Pressure

Nagano et al. Astroparticle Phys. 20 (2003) 293

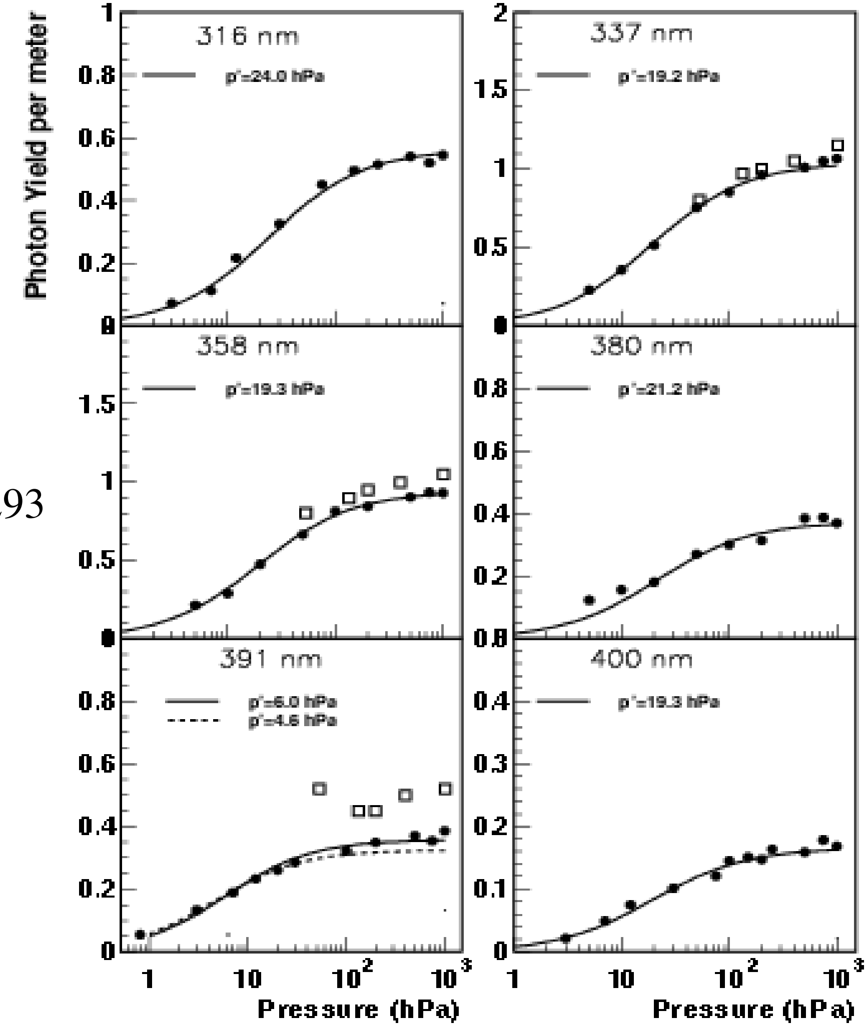

Fig. 6. The pressure dependence of ϵ in air at 20 °C. The data of Kakimoto et al. in dry air at 15 °C with 1.4 MeV electrons is plotted by open squares. Solid lines show the best fit of Eq.(10) with the value of p' as shown, as discussed in Section 4.1. The dotted line in the plot of the 391 nm dependence is the best fit excluding the four highest points.

Reconstructing The CR Energy

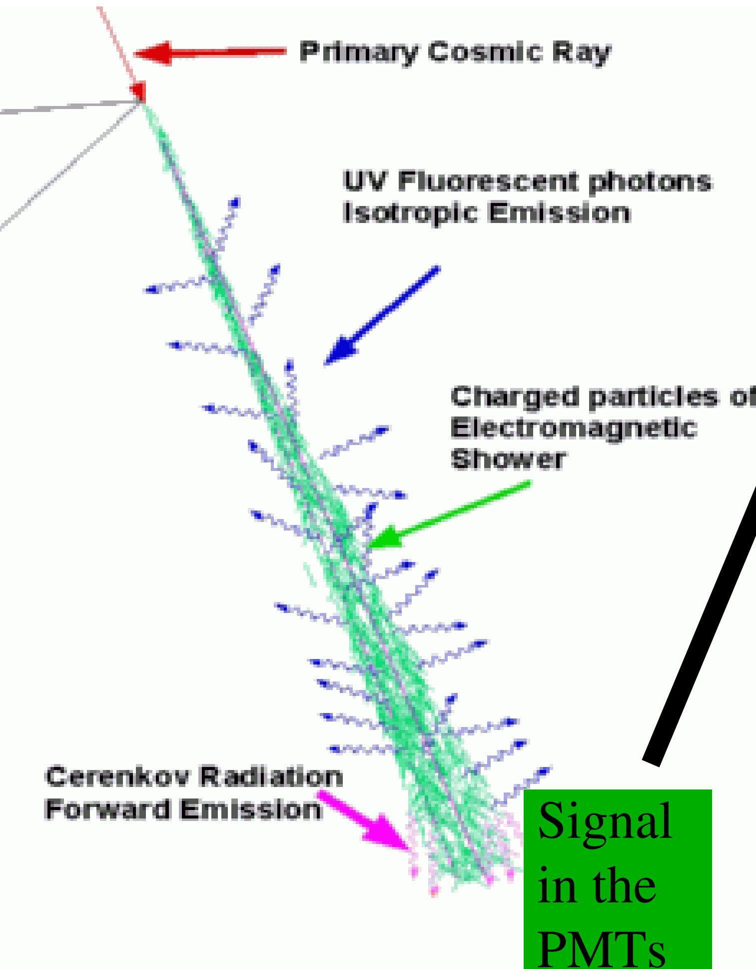

Photons at the FD

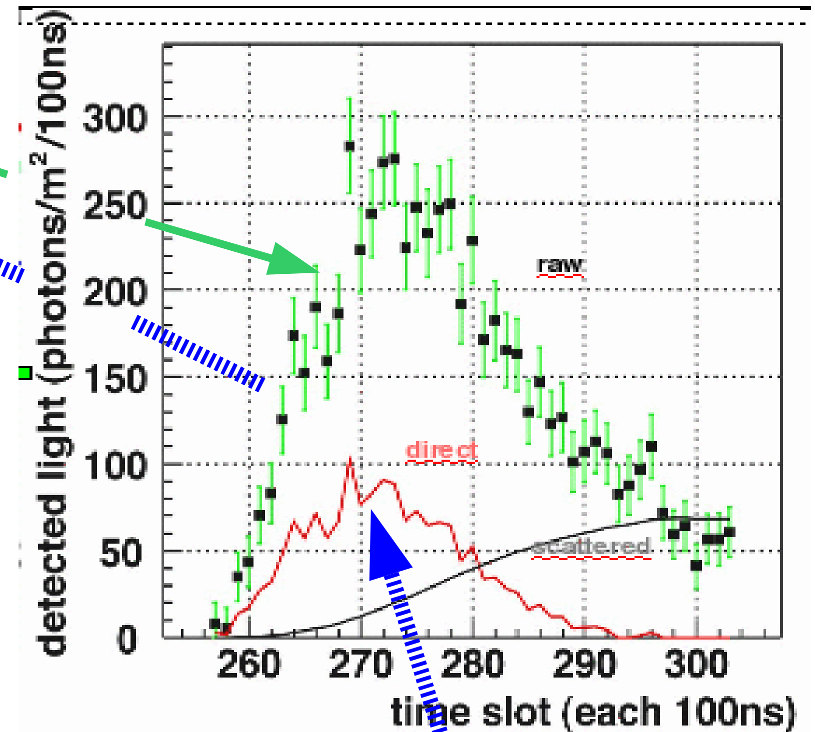

Fluorescence photons emitted at the shower axis

Signal in the PMTs

shower size profile

Estimating Cerenkov contributions

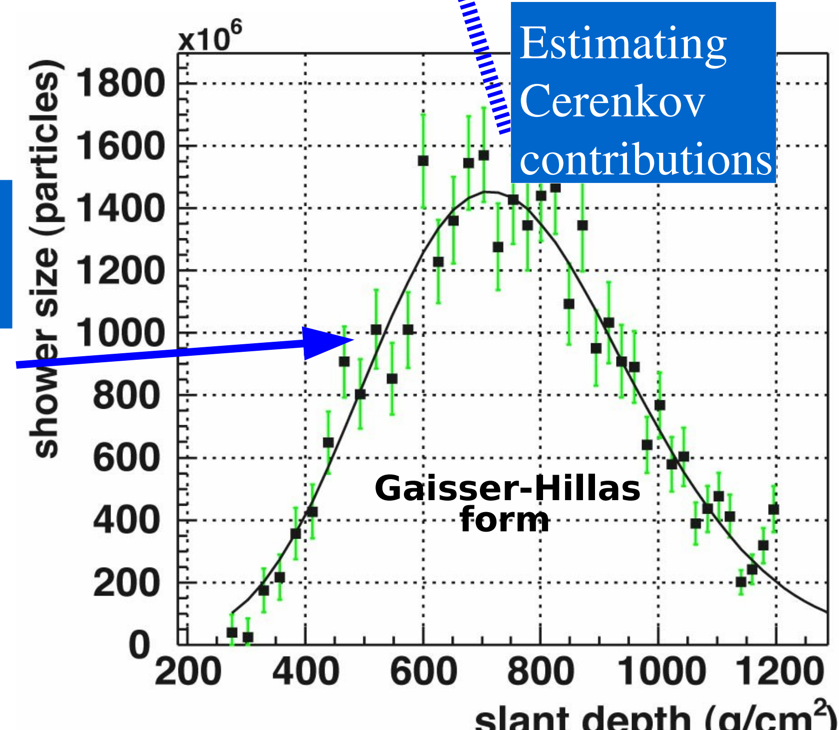

Energy deposited per slant depth

Primary CR Energy

Reconstructing The CR Energy

Not all the CR energy is deposited in the atmosphere!!

Primary CR Energy

Energy deposited per slant depth

Some muons and neutrinos from the EAS may not interact in the atmosphere and they go into the ground. The CR energy fraction that goes into the ground depends on the CR primary particle and this fraction could be between 10% (Proton) to 15% (Iron) of the total energy.

C. Song Astroparticle Physics 14 (2000) 7 - 13

Depth of Shower Maximum (Xmax)

The depth of shower maximum or Xmax is sensitive to the primary cosmic ray composition. **Lighter primaries penetrate deeper in the atmosphere** (higher value of Xmax), while **heavier particles develop earlier in the atmosphere** (smaller value of Xmax).

The value of Xmax for a given primary also has a dependence on its energy. Energetic CR are more penetrating. Measuring the mean value of Xmax of comic rays at different energies, we can determine (in a statistical basis) the abundance of lighter and heavier CR primaries.

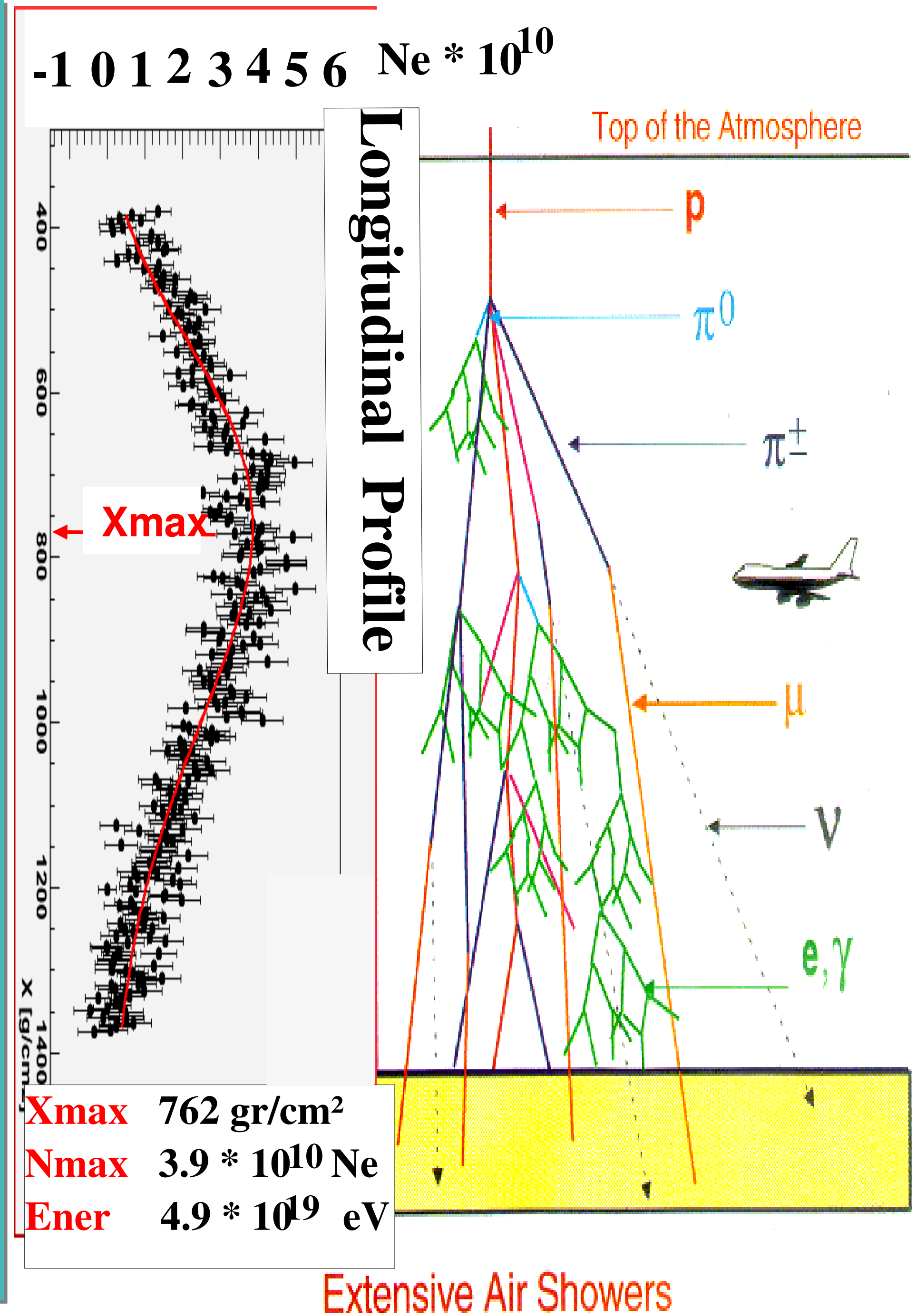

Recovering The CR Composition

Expected Xmax distributions

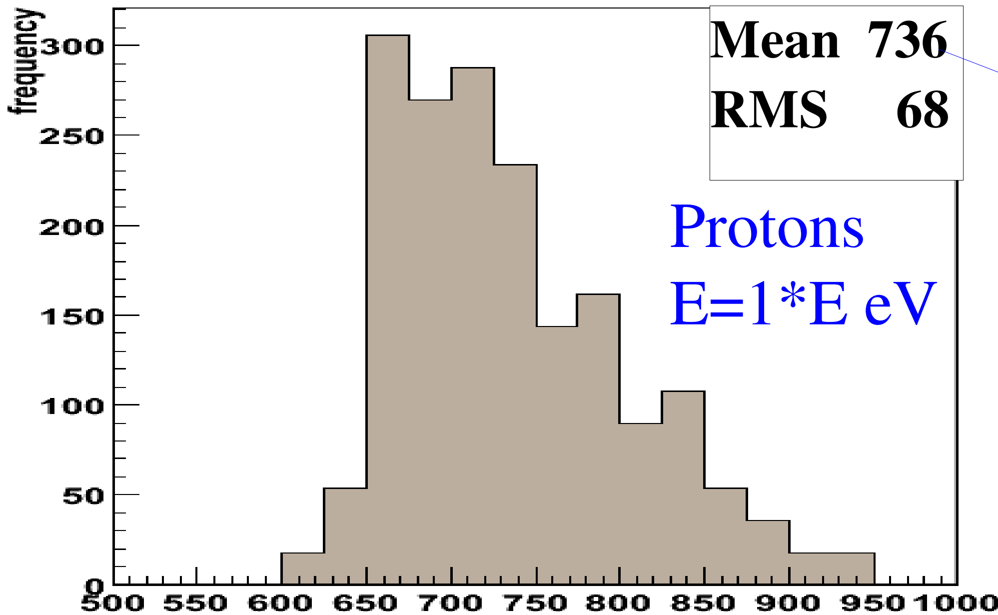

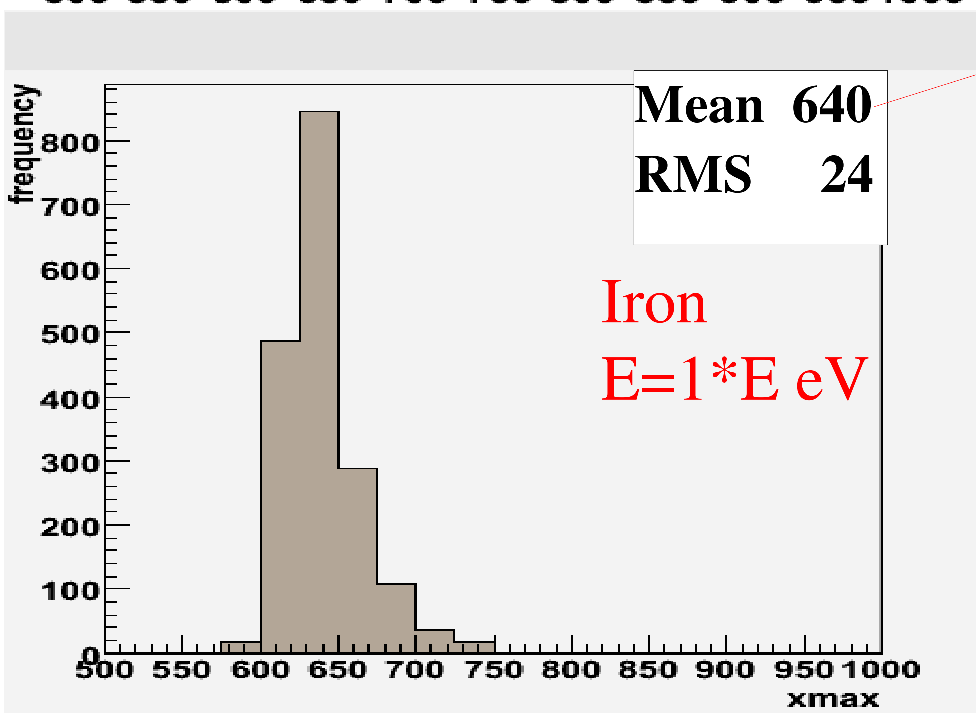

Reconstructed mean Xmax

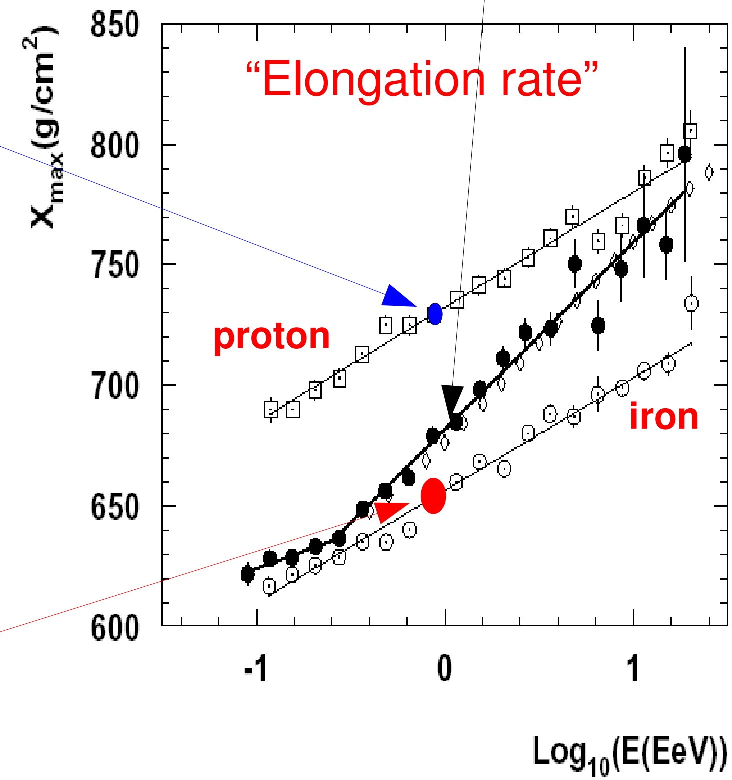

Due to natural Xmax fluctuations, the CR composition is not recovered in an event by event basis. However, statistically we can roughly estimate the fraction of photons, protons and Iron nuclei by studying the mean Xmax values and the spread of Xmax.

Important Considerations

(Atmosphere Monitoring)

The Fluorescence Technique requires some detailed knowledge of the local atmosphere.

The **atmospheric density (pressure) and temperature profiles** are important to determine the exact fluorescence yield.

The **aerosol** content in the atmosphere is important to determine the amount of fluorescence light scattered out of the PMT field of view and the amount of Cerenkov light scattered into the PMTS field of view.

The presence of **clouds** affect the propagation of fluorescence photons, and depending on the cloud location, it can make the shower to look more bright due the higher amount of scattered Cerenkov photons.

Important Considerations

(FD Calibration)

Ideally the detector needs to have an **absolute end-to-end calibration** once or twice a year and regular (every day that the detector is in operation) relative calibrations.

The **end-to-end calibration** should provide the conversion factor (calibration constant) from signal recorded in the PMT (ADC counts per unit of time) to number of photons arriving to the detector. Taking into account the efficiency of each component of the detector.

Regular **relative calibrations** should monitor the stability of the PMTs. Relative calibrations are performed at the beginning and at the end of the detector's operation.

Advantages and disadvantages of Fluorescence Detectors

Advantages

- The FD performs a calorimetric measurement of the shower energy. This means that there is not necessity for simulations of high energy showers to determine the shower energy (the energy is basically model independent).

- Depending on size of the collector mirror, the FD can observe energetic showers up to about 40 km away (large collecting area).

- The entire shower profile may be observed and Xmax can be measured with good precision.

Disadvantages

- The FD only operates during moonless nights. Therefor, it only has a 10% duty cycle.

-The weather conditions (rain, clouds, snow) affect the regular detector operation.

End

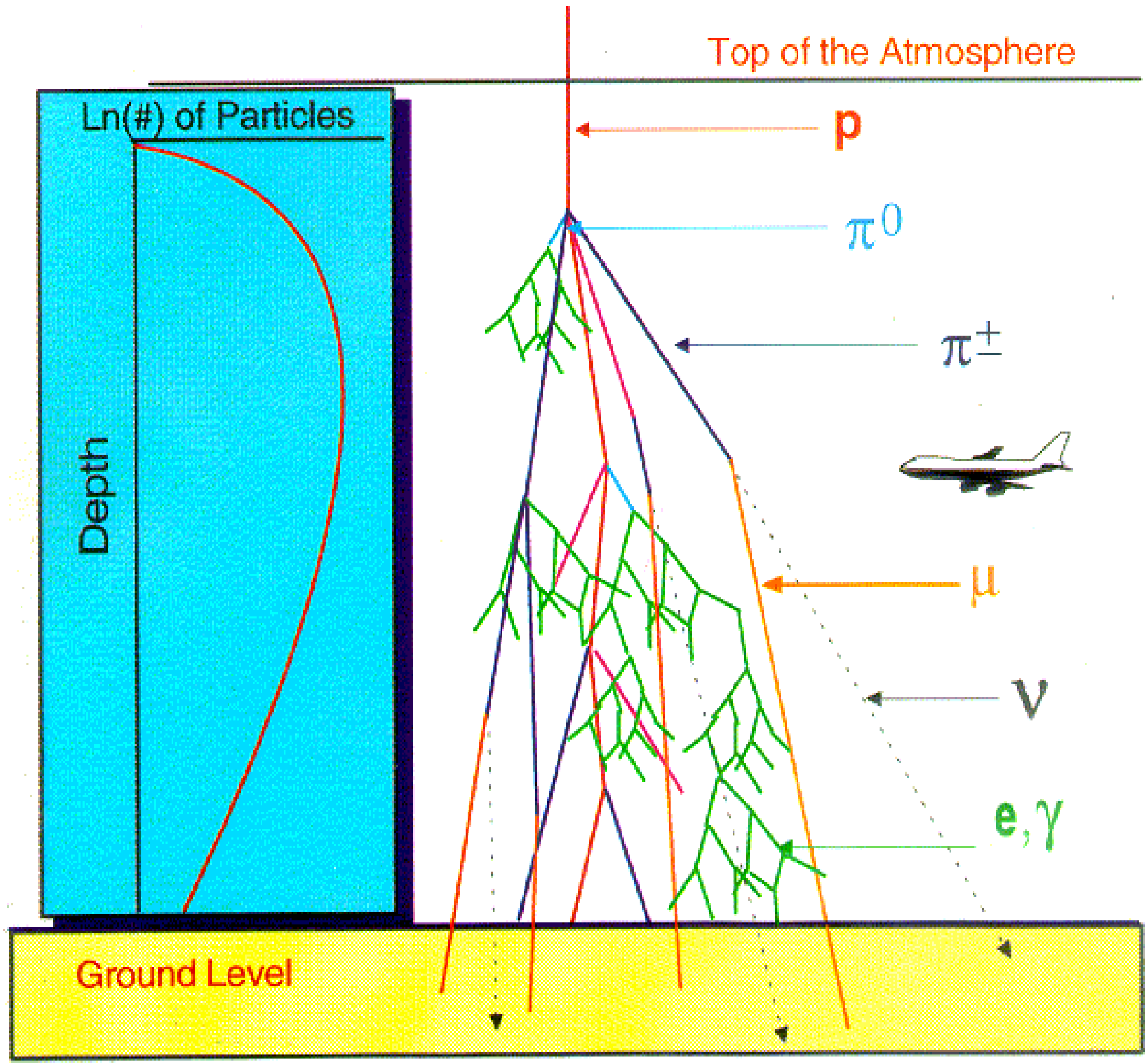

Extensive Air Showers